

# A novel artificial intelligence approach for regolith geochemical grade prediction using multivariate adaptive regression splines

Fareed Majeed<sup>a</sup>, Yao Yevenyo Ziggah<sup>b</sup>, Charles Kusi-Manu<sup>c</sup>, Bemah Ibrahim<sup>d</sup>, Isaac Ahenkorah<sup>e,\*</sup>

<sup>a</sup> Adamus Resource Limited Box 31, Esiamma, W/R, Ghana

<sup>b</sup> Department of Geomatic Engineering, University of Mines and Technology, Ghana

<sup>c</sup> Department of Geology, AngloGold Iduapriem Limited, Ghana

<sup>d</sup> Geopert Limited, Ghana

<sup>e</sup> University of South Australia, UniSA STEM, SA, 5000, Australia

## ARTICLE INFO

### Article history:

Received 28 December 2021

Revised 31 January 2022

Accepted 9 February 2022

### Keywords:

Multivariate adaptive regression spline  
Artificial intelligence techniques  
Kriging geostatistical technique  
Ashanti belt  
Geochemical grade prediction

## ABSTRACT

The necessity for applying a potent analytical regolith geochemical grade estimator is driven by the reality of mineral exploration. This is because many exploration geologists rely upon the classical geostatistical method of Kriging which oftentimes do not produce accurate predictions due to the complexity of interactions between geological features and spatial variables. In this study, a novel non-linear data-driven approach known as Multivariate Adaptive Regression Spline (MARS) is proposed as an effective predictive tool to unravel regolith geochemical complexities. The proposed MARS approach was used to predict regolith geochemical grade from a thick regolith cover in the Tarkwaian paleo-placer of the South-Western Ashanti belt in Ghana. Out of the 891 samples, the data was partitioned into 70% training (model development) and 30% testing (model validation). The proposed MARS result was compared with three other artificial intelligence techniques (i.e., radial basis function neural network, backpropagation neural network and generalised regression neural network) and kriging geostatistical technique. Based on the test results, MARS had the highest correlation coefficient ( $R = 0.9675$ ) and the least statistical error metrics ( $RMSE = 0.7791$ ,  $MAE = 0.6014$ , and  $\rho = 0.0472$ ). The implementation of the MARS approach in regolith geochemical grade estimation domain has yielded outstanding and promising results. The MARS superiority was evident in its calibration strength, prediction accuracy, robust interaction of variables and overcoming the black box system of ANN. Thus, the proposed MARS approach could be an excellent tool in regolith geochemical grade estimation workflow when fully integrated with exploration tasks.

© 2022 The Author(s). Published by Elsevier Ltd on behalf of Ocean University of China.  
This is an open access article under the CC BY license (<http://creativecommons.org/licenses/by/4.0/>)

## 1 Introduction

The future of mining and mining-related industries looks bleak as governments and investors struggle to add an ounce to existing production mines. Over the past decade, there has been a tremendous decline in exploration activities and collapse or near-collapse of existing mines. This worrying trend has not escaped the attention of the geoscience industry. Indeed, the discovery of economic mineral deposits has dwindled significantly (Barnett and Williams, 2012) hence the need to salvage the situation.

Generally, exploration is preoccupied with integrating relevant datasets and utilising various techniques to discover subtle surface

indications of mineralisation. The most pertinent decision, according to Barnett and Williams (2012), is deciding where to focus attention on the ocean of barren and prospecting areas. Accordingly, one of the most fundamental and crucial tasks in regional-scale geochemical exploration involves the delineation of exploration targets using soil, stream sediment and lithochemical geochemical data (Carranza and Hale, 1997; Cheng, 2007; Carranza, 2011; Afzal et al., 2013; Parsa et al., 2016; Ghezelbash and Maghsoudi, 2018; Ghezelbash et al., 2018; Liu et al., 2018). This will usually lead to regolith geochemical models and possibly mineral deposit discovery. Ghana located in tropical zones is endowed with thick regolith, i.e., a layer of weathered residual soil mass that covers most of the South Ashanti lode auriferous belt (Griffis et al., 2002), has proven to be a source of favourable ore enrichment (Griffis et al., 2002; Carranza et al., 2009). However, geoscientists usually are challenged with the ability to model

\* Corresponding author.

E-mail address: [isaac.ahenkorah@mymail.unisa.edu.au](mailto:isaac.ahenkorah@mymail.unisa.edu.au) (I. Ahenkorah).

and predict favourable targets for final follow-up. To circumvent the situation, the use of data mining, Geographic Information System (GIS) and geostatistical techniques have aided in geochemical data processing, grade estimation and anomaly detection (Moyeed and Papritz, 2002; Misra et al., 2007; Rossi and Deutsch, 2014; Ghandhi and Sarkar, 2016). The fundamental design and interpretation of lithochemical target generation mineral prospectivity mapping and grade predictions and estimation have been discussed in detail by various authors (Marjoribanks, 2010; Carranza and Sadeghi, 2010; Porwal et al., 2010; Chilès and Delfiner, 2011; Rossi and Deutsch, 2014; Keyan et al., 2015; Ghandhi and Sarkar, 2016).

In the last two decades, geostatistical modelling with GIS has been used to establish measures of spatial continuity or variability for ore grade estimation. This hybrid modelling has become the standard and most widely used technique for regional geochemical target generation and mineral resource estimation (Hale and Plant, 1994; Goovaerts, 1997; Isaaks and Srivastava, 1988; Isaaks and Srivastava, 1989; Hale, 2000; Chilès and Delfiner, 2011; Rossi and Deutsch, 2014; Ghandhi and Sarkar, 2016). It is a well-known fact that geostatistical modelling is known for its kriging techniques and has led to growing complexities in the handling of relationships between geological attributes (Hastie et al., 2009; Rossi and Deutsch, 2014). Despite its fame and versatility, geostatistical techniques have been plagued with certain setbacks such as its inability to model universally complex non-linear spatial relationships (Breiman, 2001; Moyeed and Papritz, 2002; Strebelle, 2002; Tahmasebi and Hezarkhani, 2012; Misra et al., 2007; Rossi and Deutsch, 2014). Besides, geostatistical techniques usually require the satisfaction of certain modelling assumptions such as stationarity, linearity and normality of dataset. Also, geostatistical modelling can be time-consuming and computationally expensive due to the complexity of cumbersome data processing (Strebelle, 2002; Leathwick et al., 2006; Misra et al., 2007; Samanta and Bandopadhyay, 2009). Moreover, in highly heterogeneous and sparse data situations, geostatistical models find it challenging to produce good results and as a result perform poorly in that regard (Samanta et al., 2004; Dutta et al., 2010).

To overcome these setbacks, there is, therefore, the need to apply an alternative method for geochemical ore grade predictions. The literature is replete with the use of several machine learning methods such as Artificial Neural Network (ANN) aimed at geochemical grade estimation and target generation (Harris et al., 2001; Brown et al., 2000; Harris et al., 2003; Porwal et al., 2003; Nykänen, 2008; Carranza and Sadeghi, 2010; Oh and Lee, 2010; Ibrahim et al., 2021) and ore grade estimation (Skabar, 2005; Samanta and Bandopadhyay, 2009; Tahmasebi and Hezarkhani, 2010). The suitability of the ANN has increased its application to geochemical data processing, analysis, interpretation and detection of geochemical anomalies due to its strength in processing non-linear variable relationships. While ANN requires extensive datasets, its training and design are computationally expensive and sometimes the results get stuck in local optima due to the gradient descent training algorithms used. In addition to that, ANN black box system has made it mathematically "unattractive" because the functional relationship between input and target variables cannot be established between the modeller and the user (Breiman, 2001; Leathwick et al., 2006). In view of these mathematical inconveniences in ANN, several researchers have adopted other machine learning techniques such as Support Vector Machine (SVM) (Zuo and Carranza, 2011; Abedi et al., 2012), Random Forest (RF) (Rodriguez et al., 2015; Carranza and Laborte, 2016), Extreme gradient boosting (Ibrahim et al., 2021), Decision tree (Reddy and Bonham-Carter, 1991; Chen et al., 2014) and hybrid ANN techniques (Adaptive Neuro Fuzzy Inference System (ANFIS), genetic algorithm-ANN (GA-ANN). These methods have been pro-

posed by various researchers and have proven their strength over the ANN methods in ore grade estimation (Samanta et al., 2004; Porwal et al., 2004; Mahmoudabadi et al., 2009; Tahmasebi and Hezarkhani, 2009; Yu et al., 2012; Chatterjee et al., 2010).

Zuo (2017) stated that machine learning has been applied in geosciences but in a limited scope and thus more applications to demonstrate its advantages and uniqueness in solving complex integrated geological datasets should be explored. This study proposes the Multivariate Adaptive Regression Splines (MARS) developed by Friedman (1991) as a novel alternative predictive tool for regolith geochemical grade estimation. The proposed MARS approach (Smith, 1982; Friedman, 1991) is a specialised form of multivariate regression algorithms that builds hierarchical models using stepwise selection and a set of basis functions. MARS can produce data-driven, localised multiple non-linear regression models wherein each region, a simple hyperplane is built and linked to each other. In addition, the MARS does not impose any underlying modelling assumptions on the dependant and predictor variables, hence, does not require class relationships on the predictor-dependant variables of interest (Quirós et al., 2009; Hastie et al., 2009).

The MARS has demonstrated its robustness against many ANN methods due to its exceptional analytical speed and intuitive capabilities that avoid fine-tuning of several parameters and slow convergence, which has been the case of ANN (Abraham et al., 2000; Moisen and Frescino, 2002; Yang et al., 2003; Yang et al., 2004; Leathwick et al., 2005). In addition to that, the MARS approach overcomes the black box system of ANN by providing a functional relationship between response and explanatory variables. Despite the widespread use of MARS and other machine learning techniques in geosciences, the situation is even alarming with respect to the six principal auriferous gold Belts in Ghana (Griffis et al., 2002), where the strength of MARS and other machine learning techniques, in general, are yet to be explored in the potentials of Ghana's rich greenstone/volcanic gold deposits. Therefore, the proposed MARS technique in this study is targeted at providing a fast, timely, and reliable regolith geochemical grade estimation, with minimum prerequisite for modelling skills and assumptions.

The simplified computational and functional capabilities of MARS (Hastie et al., 2009) as a proposed technique was tested against the benchmark machine learning methods of Radial Basis Function Neural Network (RBFNN), Backpropagation Neural Network (BPNN) and Generalised Regression Neural Network (GRNN) to demonstrate its robustness and easy interpretability of predicted results. Furthermore, this study compares the predictive capabilities of machine learning algorithms (i.e., MARS, RBFNN, BPNN and GRNN) to the classical geostatistical modelling technique of ordinary kriging.

It is widely known that regolith mapping logging codes contain numerous categorical variables, which are mostly subjective. Some of these geological features are alteration, weathering, lithological codes and oxidation. To overcome the issue of subjectivity, this study focuses on a data-driven approach, using the spatial dataset of Easting (E), Northing (N) and Elevation (Z) that define the positions of the various sample points as the input variables and gold (Au) value as the output. This study uses MARS as a novel technique to improve the prediction accuracy of interaction between Au and spatial features (E, N, Z) within the placer environments. This will be achieved by: (a) inspiring confidence and reliability of MARS as a useful universal data-driven model for regolith geochemical grade estimation; (b) accurately predicting Au values within regolith geochemical features critical for the Tarkwaian paleo-placer exploration of the South-Western Ashanti belt; and (c) demonstrate the robustness of MARS models against other benchmark methods (BPNN, RBFNN and GRNN) investigated.

## 2. Geological setting

Ghana is predominantly underlain and hosted by metamorphosed greenschist rock of the paleoproterozoic (ca. 2300–1900 Ma) age (Boher et al., 1992; Taylor et al., 1992; Davis et al., 1994; Oberthür et al., 1998; Allibone et al., 2002) and related to Eburnean orogenic cycle (Griffis et al., 2002). Much of the historical and detailed description of the geological and structural setting of Ghana is provided in these studies (Junner, 1940; Kesse, 1985; Hirdes et al., 1993; Loh and Hirdes, 1996; Griffis, 1998). The study area falls within the Tarkwaian paleoplacer within the prolific South-Western Ashanti orogenic lode gold belt system.

### 2.1. Geology and mineralisation style of the Tarkwaian

The study area is located within the Tarkwaian group, which forms part of the West African Craton. It is covered largely by the Birimian volcanic and metasediments. The Birimian Supergroup underlining the Tarkwaian Group consists of metamorphosed lava and pyroclastic rocks, which contains abundant grey wacke (meta siltstone and sandstone), phyllites and intrusive rocks. The Tarkwaian group consists of a thick sequence of clastic metasedimentary rocks that have suffered low grade regional metamorphism, shearing and altering by hydrothermal solution (Kesse, 1985). The higher grades are uncommon and are often associated with intrusive rocks. Locally, the mine is situated along the southern end of the Tarkwa syncline (basin) of the Tarkwaian Group. Gold mineralisation occurs in a sedimentary sequence known as the Banket Formation.

The Banket Reef zone comprises a sequence of individual beds of quartz conglomerates (Banket beds), breccia conglomerates, meta-sandstones (quartzite) and grits. All the known gold mineralisation is associated with the conglomerates and is found within the matrix that binds the pebbles together (Griffis et al., 2002). The Tarkwaian group consists of a thick sequence of clastic meta-sedimentary rocks that have suffered low-grade regional metamorphism, shearing and altering by hydrothermal solution (Kesse, 1985). The higher grades are uncommon and are often associated with intrusive rocks. The Tarkwaian group is subdivided into four main groups: Kawere Formation, Banket Formation, Tarkwa Phyllite Formation and Huni Formation (Fig. 1). The Basal Kawere Group is predominantly polymictic, poorly sorted sandstone and conglomerates and varies in thickness between 250 m and 700 m, which contain low economic gold mineralisation (Ewusi et al., 2017).

The overlying Banket Formation comprises conglomerates, made up of volcanic clasts and Birimian quartz pebbles, with intercalated cross-bedded sandstones. The Banket Formation hosts the Tarkwa Placer gold deposit (<100 m thick gold zone), attains an estimated maximum thickness of 600 m and grades upwards into the Tarkwa Phyllite Formation, which is about 400 m thick. The Phyllites grades conformably into the uppermost Huni Formation, which consists of approximately 1400 m thick sequence of sandstones with interbedded phyllites and quartzites, intruded by minor dolerite sills (Kesse, 1985; Strogen, 1991; Griffis et al., 2002; Pigois et al., 2003; Perrouty et al., 2012).

## 3. Overview of methods

In this section, the theoretical concept of the proposed MARS technique is briefly presented. Also presented are the Kriging technique and the various benchmark machine learning techniques (BPNN, RBFNN, and GRNN), which have been successfully applied to grade estimation.

### 3.1. Multivariate adaptive regression splines

MARS is a form of regression analysis introduced by Jerome Friedman for solving classification and regression problems (Friedman, 1991). The method can select and transform variables automatically and can easily recognise and identify their potential interactions. The MARS approach fits the stepwise linear basis function of the form  $(x-a)_+$  and  $(a-x)_+$  as shown in Eq. (1).

$$Y = (x - a)_+ = \begin{cases} x - a, & \text{if } x > a \\ 0, & \text{otherwise} \end{cases}; \quad Y = (a - x)_+ = \begin{cases} a - x, & \text{if } a > x \\ 0, & \text{otherwise} \end{cases} \quad (1)$$

where “+” means positive part and  $a$  is an arbitrary threshold value. Here, the MARS breaks the data into step-functions having a knot at the value  $a$ , that imposes a locally non-linear relationship. These two functions are direct mirror pairs such that a collection of basis functions,  $C$ , of non-linear pattern for every input  $x_j$  with an observable knot of  $x_{ij}$  of that input (Eq. (2)) is formed in a continuous chain of functions (Hastie et al., 2009).

$$C = \{(x_j - a)_+, (a - x_j)_+\}, \quad a \in \{x_{1j}, x_{2j}, \dots, x_{Nj}\}; \quad j = 1, 2, \dots, p \quad (2)$$

The MARS model building involves the forward and backward selection stages. In the forward stage, MARS builds a flexible piecewise model by dividing the solution space into various intervals of predictor parameters which are hierarchical (Hastie et al., 2009). This is accomplished by building knots with an analytical construct known as the basis function. The knot building stops after a specified upper limit is attained. Usually, the initial MARS model typically overfits the data (with so many knots) so a later backward pruning is followed to delete the redundant knots. The MARS final predictive model thereby has the general form as expressed in Eq. (3).

$$f(x) = \beta_0 + \sum_{m=1}^M \beta_m h_m(x) \quad (3)$$

where  $h_m(x)$  is the  $m^{th}$  basis function,  $\beta_0$  is the constant term,  $M$  is the number of basis functions,  $\beta_m$  is the coefficient corresponding  $h_m(x)$ . The final stage involves determining the optimal model of which MARS typically uses the Generalised cross-validation (GCV) criterion (Friedman, 1991; Hastie et al., 2009; Kuhn and Johnson, 2013) on the data, defined in Eq. (4).

$$GCV(\lambda) = \frac{\sum_{i=1}^n (y_i - \hat{h}_\lambda(x_i))^2}{\left(1 - \frac{P(\lambda)}{n}\right)^2} \quad (4)$$

where  $\lambda$  is the number of terms,  $y_i$  is the  $i^{th}$  response variable,  $\hat{h}_\lambda(x_i)$  is the fitting response,  $P(\lambda)$  is the effective number of parameters in the model and  $n$  is the number of observations. It must be noted that  $P(\lambda)$  is generally related to the number of basis functions,  $d$  is the penalty term of the model, and  $k$  represents the flexibility or complexity of the model. It follows that  $P(\lambda) = r + kd$ . According to Hastie et al. (2009),  $k$  is defined between  $2 < k < 3$ .

### 3.2. Backpropagation neural network

The BPNN architecture consists of input, hidden and output arranged in a feed-forward manner (Fig. 2). The technique can also be described as a universal nonlinear multilayered feed-forward function approximator (Ahmadian, 2016) that adapt weights of layer connections continuously after each training process. The weight adjustment is based on the error difference between the predicted and expected results. Each layer initialises with a weight

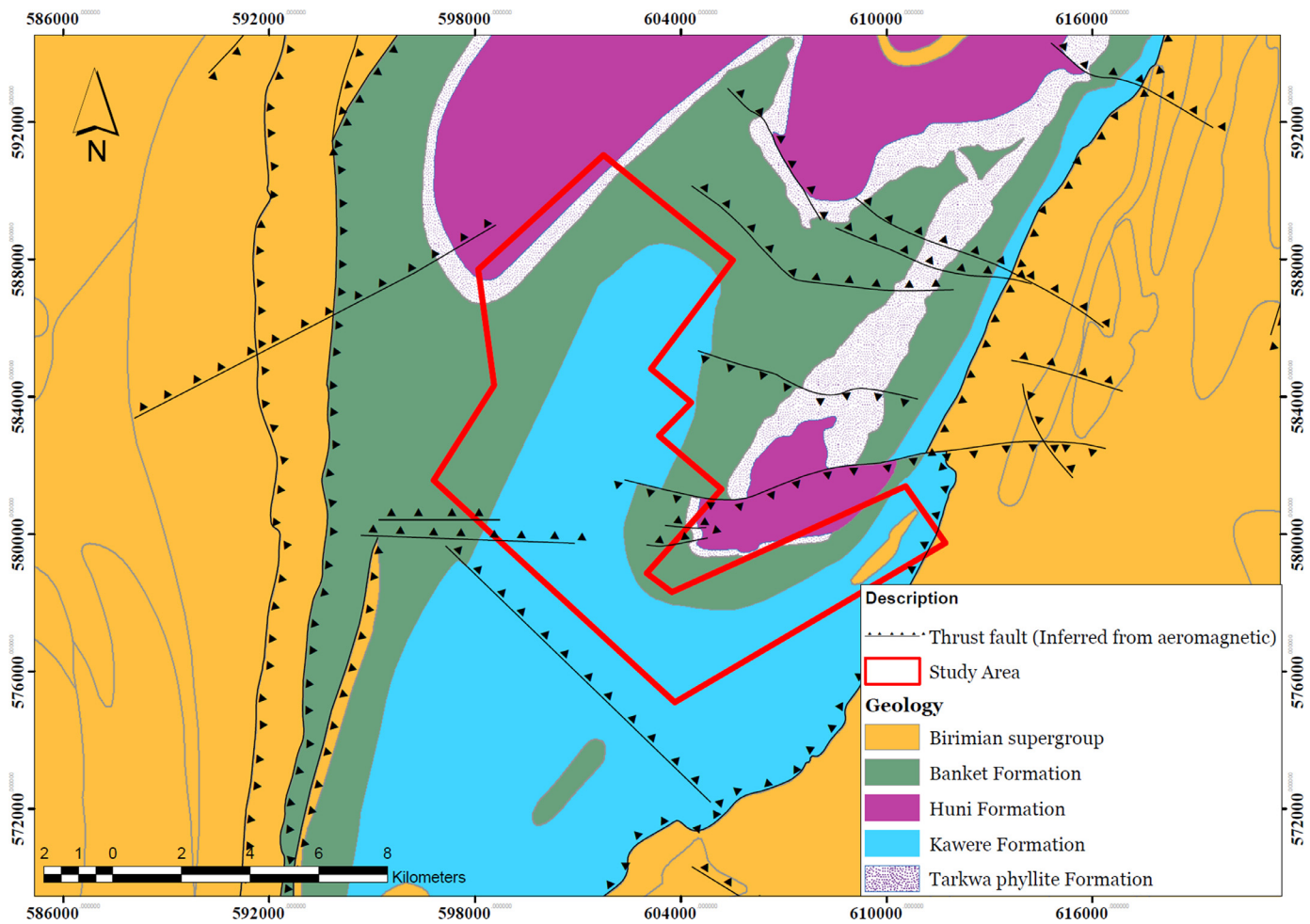


**Fig. 1.** Simplified stratigraphic sequence map and geological map of south-western Ghana.

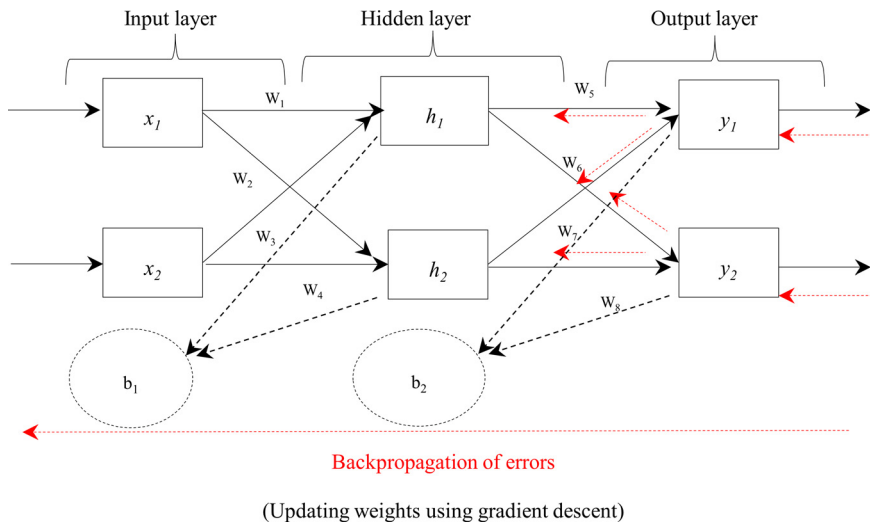


**Fig. 2.** Backpropagation neural network architecture.

matrix ( $w_{ij}$ ), a bias ( $b_i$ ) and an output, ( $y_i$ ) vector. Typically, the computational process of the BPNN involves two stages (i.e., the forward and backward phase).

The forward phase involves computing the signal of the output neurons. This is achieved through a systematic sequence of inputs, applying weights and “squashing” with activation function and given predicted signal. Here, each neuron receives a set of

inputs ( $x_i$ ) to the input layer, performs a dot product with the weights matrix, bias vector ( $b_i$ ) and transfer it into the hidden layer. In the hidden layer, an activation function is applied to the outputs from the input layer. In this study, the hyperbolic tangent transfer function which gives values within the range of -1 to 1 (Karlik and Olgac, 2010; Mueller and Massaron, 2016) was used in the hidden layer. The results from the hidden layer are then sent

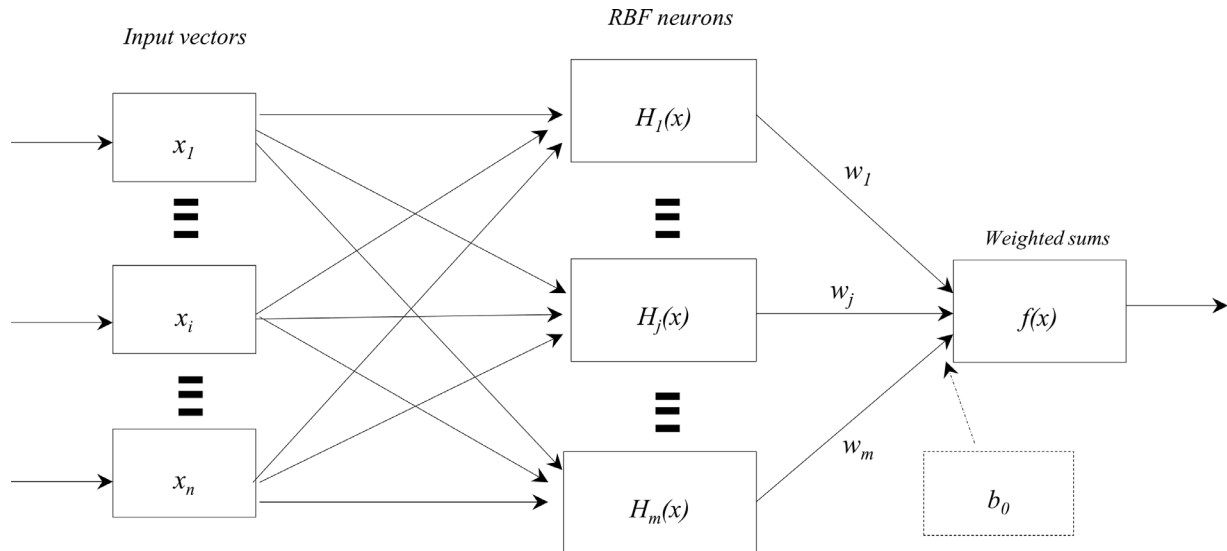


**Fig. 3.** Radial basis function neural network architecture.

to the output layer for further processing. The same computation process in the hidden layer is repeated for the output layer neurons to produce the predicted outputs.

The backward phase involves computing error (difference between predicted and desired outputs) and backpropagating (reversing) to modify the connected weights, starting from output layers with the objective of minimising the error function (Fig. 2). The backpropagating process iterates until the error margin reached an acceptable limit.

### 3.3. Radial basis function neural network

RBFFNN is a form of multilayered feed-forward network. It was originated from Powell (1977), introduced and formulated by Broomhead and Lowe (1988), and Moody and Darkin (1989). Its versatility and uniqueness in solving function estimation, pattern recognition and classification problems have been demonstrated by several authors (Poggio and Girosi, 1990; Chen et al., 1991; Bishop, 1991; Musavi et al., 1992; Chang and Lippmann, 1993; Haykin, 1994; Roy and Miranda, 1995; Bishop, 1995; Behnia, 2007; Quirós et al., 2009; Patra et al., 2015). Specifically, the RBFFNN has also been applied to ore grade estimation (Kapageridis and Derby, 1998) and prospectivity mapping (Nykänen, 2008). The RBFFNN architecture consists of an input layer, a non-linear hidden layer activation function called radial basis function (RBF) and a linear activation function for the output layer (Fig. 3). The RBF consists of only one hidden layer that contains the transfer function, unlike the BPNN where several hidden layers can be used.

The input variables correspond to the number of neurons in the input layer. First, the input neurons, \$x\_n\$, feed the values to the hidden layer in a vector space. Now the input vector is connected to the computational neurons in the hidden layer with Gaussian radial basis activation function (Eq. (5)), which is inversely related to the distance from the centers of neurons (Hagan et al., 1996; Haykin, 1999).

$$\varphi(x) = \exp\left(-\frac{\|x_i - c_m\|^2}{2\sigma_m^2}\right), \quad m = 1, 2, \dots, q \quad (5)$$

where \$\varphi\$ is the Gaussian RBF, \$\sigma\$ is the spread (variance) responsible for the smoothness of the activation function, \$x\_i\$ is the input vector, \$c\_m\$ is the centre vector of the \$m^{th}\$ activation centre and \$\|x\_i - c\_m\|\$ is the distance between the input and the centre of the function. The \$\sigma\$ and \$c\_m\$ in each RBF dimension, network

weight parameters of the output layer and the optimal number of hidden layer neurons are determined during the network training Haykin, 1999). Here, the centers of the RBFs of the network are specified through either gradient descent learning, random selection (Broomhead and Lowe, 1988; Poggio and Girosi, 1990), or self-organising methods such as the k-means clustering technique (Moody and Darkin, 1989). The Euclidean norm \$\|\cdot\|\$ is used to express the distance of data points to the centre of each neuron (this is within the same dimensional space as the inputs). The respective weights, centers and the spread are trained using the following learning rules as given in Eqs. (6)-(8).

$$w_{mn}(k+1) = w_{mn}(k) + \eta e(k) h_m(k) \quad (6)$$

$$c_{mi}(k+1) = c_{mi}(k) + \eta e(k) w_{mn} h_m \frac{\|x_i(k) - c_{mi}(k)\|}{\sigma_m^2(k)} \quad (7)$$

$$b_m(k+1) = b_m(k) + \eta e(k) w_{mn} h_m \frac{\|x(k) - c_m(k)\|^2}{\sigma_m^3(k)} \quad (8)$$

where \$\eta\$ is the learning rate, \$e(k)\$ is the error in \$k^{th}\$ sampling, \$w\_{mn}\$ is the connect weight between \$n^{th}\$ output node, \$m^{th}\$ is the basis function and \$b\_m\$ is the width vector. The network's weight parameter is computed and updated for each neuron from the calculated distance using the recursive least squares parameter identification technique (Nekoukar and Beheshti, 2010; Senapati and Dash, 2013). Finally, predictions are made by the weighted sum of the RBFs' outputs and weights of each neuron and optimal spread. Hence, the outputs of the hidden layer are weighted \$w\_m\$ and output function \$f(x)\$ (Haykin, 1999) is computed as given in Eq. (9).

$$f(x) = \sum_{m=1}^q w_m \varphi(\|x_i - c_m\|) + b \quad (9)$$

where \$b\$ is bias vector with weight nodes, \$w\_1, w\_2, \dots, w\_q\$.

### 3.4. Generalised regression neural network

GRNN was first introduced by Specht (1991) and related to the probabilistic neural classifier. A GRNN is similar to RBFFNN with slight variation in its architecture and computational procedures (Ahmadian, 2016; Hannan et al., 2010). For example, within the training dataset, the GRNN set one neuron to each sample with a very fast learning rate because it does not require an iterative

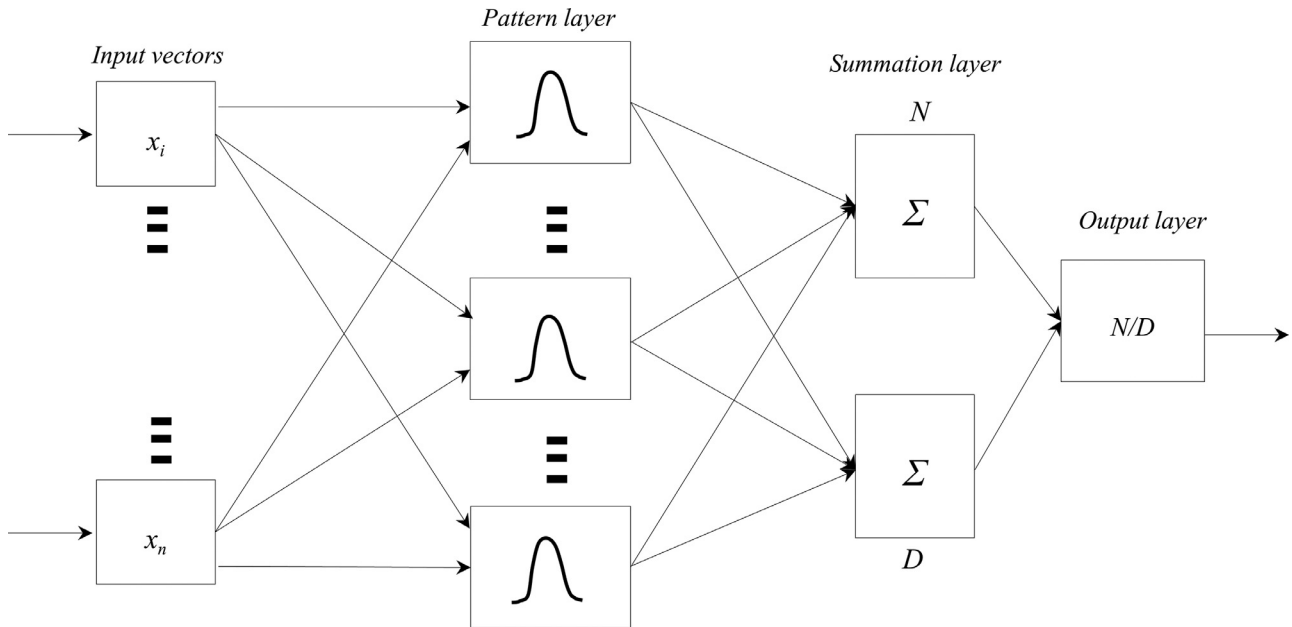


Fig. 4. Generalised regression neural network architecture.

procedure to produce results as has been observed in the Probabilistic Neural Network (PNN), RBFNN and BPNN (Hannan, 2010). This enables the GRNN to be less sensitive to the training dataset (Subramanian and Saraswathi, 2012). A GRNN network architecture consists of four basic layers: input layer, pattern layer, summation layer and output layer, as shown in Fig. 4.

The first layer, which is only a distribution unit, is fully connected to the pattern layer with one more node than the output layer. Each sample within the training data will influence every point that is being predicted by GRNN. The pattern layer, which is the first hidden layer, takes on the scaled measurement variables  $x$  from the input layer. The pattern layer consists of an  $N$  number of training samples where each node is represented by a  $x_i$  input vector. The input vector is associated with the assigned vector with the  $j^{th}$  training sample data point. Within each node, the input vector is subtracted from the assigned vector to the node,  $x_i$ , that is squared by the node. The result is then fed into a non-linear radial basis kernel function (Hannan et al., 2010). The outputs from the pattern hidden layer are passed onto the summation layer (second hidden unit).

The summation layer has two parts, the Numerator ( $N$ ) and Denominator ( $D$ ) Eq. (11)). The  $N$  part contains the summation of the multiplication of the first hidden layer outputs and the observed training output,  $y_i$  corresponding to  $x_i$ . The input of the second node ( $D$ ) is the summation of the first hidden layer activation function. Finally, the fourth layer is the output layer which receives the two outputs from the summation layer and merely divides ( $N/D$ ) to yield an estimate or prediction result of  $f(x)$  (Jang et al., 1997). The GRNN can generalise for new inputs after adequately learning from the training datasets. The GRNN output is computed using Eqs. (10) and (11).

$$d_i^2 = (x - x_i)^T (x - x_i) \quad (10)$$

$$f(x) = \frac{\sum_{i=1}^n y_i \exp\left(-\frac{d_i^2}{2\sigma^2}\right)}{\sum_{i=1}^n \exp\left(-\frac{d_i^2}{2\sigma^2}\right)} = \frac{N}{D} \quad (11)$$

where  $e^{-d_i^2/2\sigma^2}$  is the Gaussian activation function,  $d_i^2$  is the Euclidean distance between the training vector,  $x_i$ , and the input sample  $x$ , and  $\sigma$  is the spread (variance) responsible for the smoothness of the GRNN.  $f(x)$  is the predicted outputs of the network.

### 3.5. Kriging interpolation

Kriging resembles a non-parametric local fitting model that restricts the mapping of the model through variogram structure to a neighbourhood of datasets (Misra et al., 2007; Rossi and Deutsch, 2014). In kriging, the prediction of an unknown value at a location is obtained by linearly weighting the data points near to that particular location using the variogram structure of the spatial attribute (Moyeed and Papritz, 2002; Misra et al., 2007; Rossi and Deutsch, 2014; Ghandhi and Sarkar, 2016). amongst the numerous kriging estimators, the most versatile and common estimation technique is ordinary kriging (Rossi and Deutsch, 2014), although different kriging methods are becoming popular in recent years. By construction, kriging and its variants is a minimum error estimator (Rossi and Deutsch, 2014), and according to Srivastava (1987), no other set of weights can estimate lower variance than kriging. While least-squares optimisation is the valuable property of kriging, there are cases where minimum variance may be the wrong optimisation criteria to use (Srivastava, 1987). In this study, the most widely used ordinary kriging estimation method was used. Eq. (12) expresses the generalised form of the kriging interpolation technique.

$$\hat{z}(x_0) = \sum_{i=0}^n (\lambda_i z(x_i)) \quad (12)$$

where  $\lambda_i$  is an unknown weight for the measured value at the  $i^{th}$  location,  $x_0$  is the prediction location,  $n$ , denotes the number of measured values,  $\hat{z}(x_0)$  is the estimate at an un-sampled location,  $x_i$  is the measured value at the  $i^{th}$  location.

In ordinary kriging, the  $\lambda_i$  does not depend only on the difference in distance between predicted and measured locations, but on the total spatial arrangements of the measured locations. Typically, kriging interpolation is achieved through (i) estimating statis-

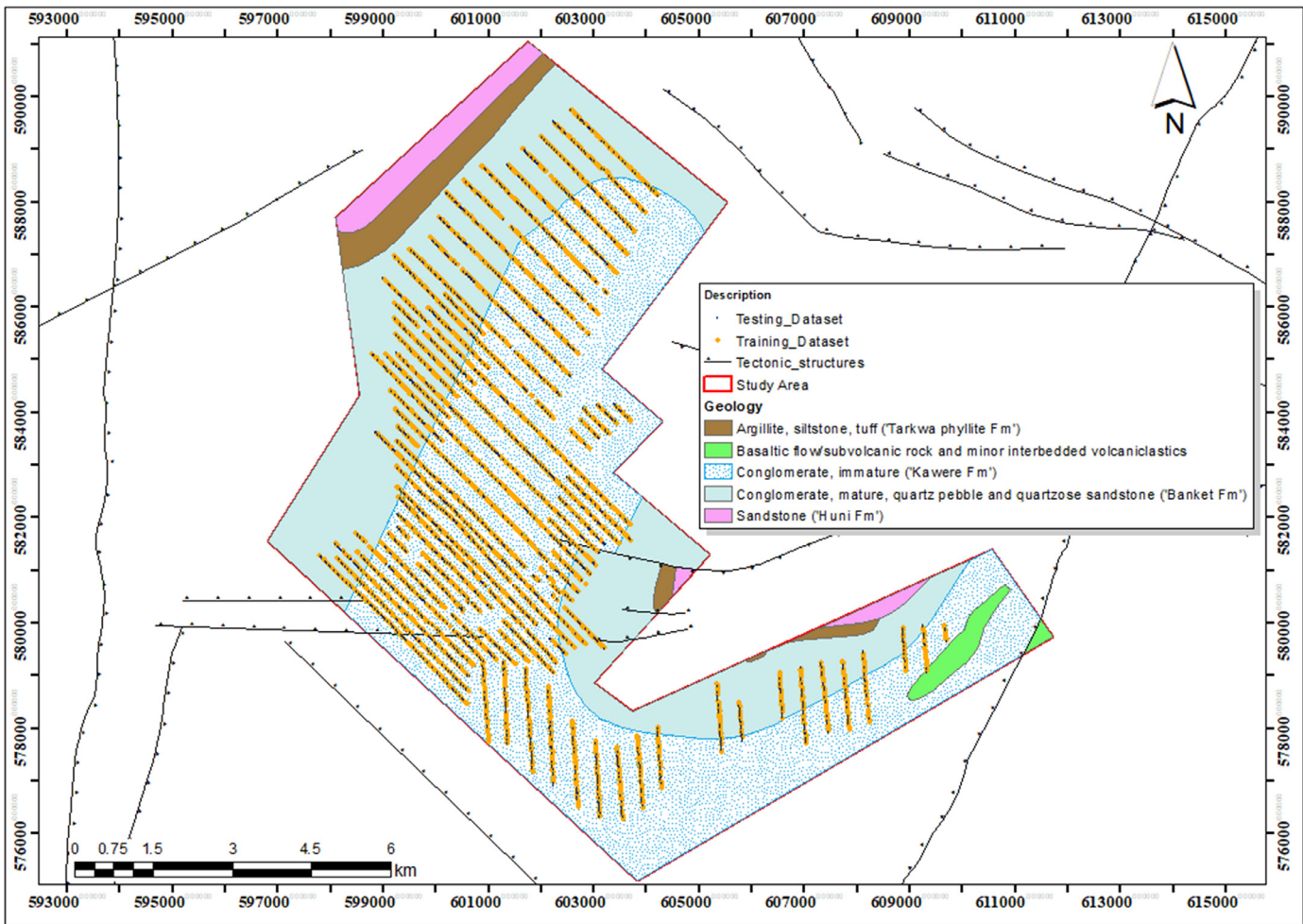


Fig. 5. Sampling points of the study area showing training and testing datasets.

tical dependence using variography and covariance functions and (ii) predicting unknown locations. Variography, however, is used to fit a model for use in kriging interpolation. The semi-variogram can be written in the form (Eq. (13)):

$$\gamma(x_0) = \frac{1}{2N(x_0)} \sum_{i=0}^n [z(x_i) - z(x_i + x_0)]^2 \quad (13)$$

where  $N(x)$  is the number of pairs for lag separation,  $x$ . Fitting empirical semi-variogram models involves function approximators such as Gaussian, spherical, linear, exponential and circular models. The spherical model is the most commonly used variogram model (Rossi and Deutsch, 2014; Haldar, 2013) due to its positive definite functions. In this study, we used the spherical semi-variogram model (Eq. (14))

$$\gamma(x_0) = \begin{cases} 0, & x_0 = 0 \\ k_0 + k, & x_0 > \alpha \\ k_0 + k \left( \frac{3x_0}{2\alpha} - \frac{1}{2} \left( \frac{3x_0}{2\alpha} \right)^3 \right), & 0 < x_0 \leq \alpha \end{cases} \quad (14)$$

where  $k_0$  is the nugget effect/constant (natural or analytical error),  $k_0 + k$  is the sill (total variance where the empirical variogram appears to level off),  $k$  is the structure variance and  $\alpha$  is the range (distance where maximum variability between samples is reached).

#### 4. Statistical evaluation of model performance

In this study, various performance measures were used as a criterion for ranking and evaluating the viability of the developed models. Four statistical evaluating parameters namely: Correlation Coefficient ( $R$ ), Root Mean Squared Error (RMSE), Mean Absolute Error (MAE), and Correlation Index ( $\rho$ ) were considered (Smith, 1982; Friedman, 1991; Hastie et al., 2009). These statistical performance metrics are expressed mathematically (Asuero et al., 2006; Milani and Benasciutti, 2010; Gandomi et al., 2011; Savaux and Bader, 2015; Chai and Draxler, 2014; Gandomi et al., 2015; Hasanipanah et al., 2016) in Eqs. (15)-(18).

$$MAE = \frac{1}{N} \sum_{i=1}^N |A_i - E_i| \quad (15)$$

$$RMSE = \left( \frac{1}{N} \sum_{i=1}^N (A_i - E_i)^2 \right)^{1/2} = \sqrt{MSE} \quad (16)$$

$$R = \frac{\sum_{i=1}^N (A_i - \bar{A})(E_i - \bar{E})}{\left( \sum_{i=1}^N (A_i - \bar{A})^2 \right)^{1/2} \left( \sum_{i=1}^N (E_i - \bar{E})^2 \right)^{1/2}} \quad (17)$$

$$\rho = \frac{RRME}{R + 1} \quad (18)$$

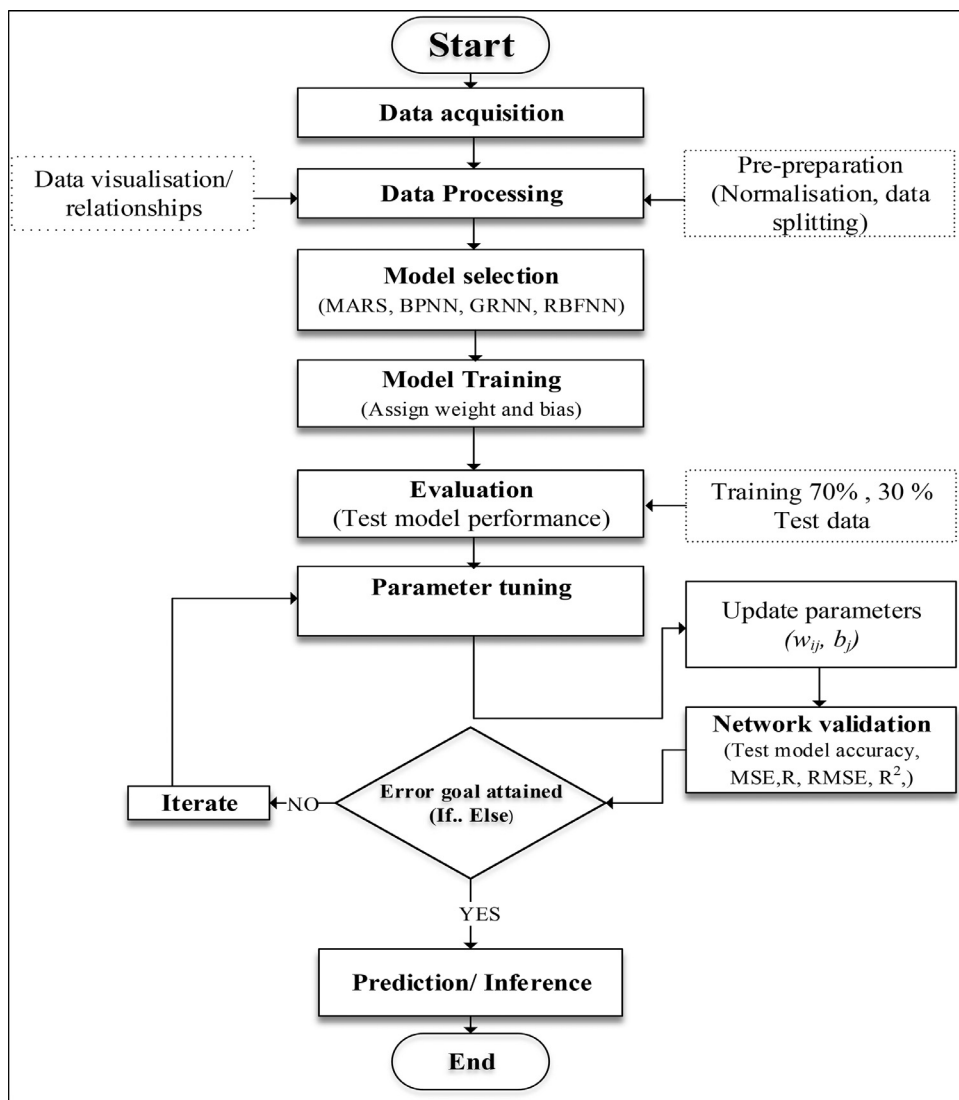


**Fig. 6.** Model-building flowchart.

where  $\bar{A}$  is the mean of the measured values  $A_i$ ,  $\bar{E}$  is the mean of the predicted  $E_i$ ,  $N$  is the total number of samples and RRME is the Relative Root Mean Square.

## 5. Results and discussion

### 5.1. Data acquisition and pre-processing

Litho-geochemical surveys are usually undertaken to target areas for the advanced stage. The surveys typically involve the collection of soil, rock and/or stream sediment samples. A total of 891 soil sediment samples were taken from the study area of about 54 sq. km on 20 m spacing sampling points at an average depth of 0.8 m (Fig. 5). This district-scale soil geochemical project was undertaken to delineate high prospectivity zones. The grid line spacing was generally 200 m. The traverse lines were orientated on NW-SE bearing across the regional lineation trends (Fig. 5). The samples were analysed for gold using aqua-regia digestion low level ( $2 \leq \text{limit} \leq 1000 \text{ ppb}$ ) technique. Aqua regia is commonly used because it dissolves elemental gold as well as breakdown iron and manganese oxides, oxy-hydroxides, carbonates, sulphates, sulphides and many types of clay. It will not release elements or minerals included within quartz (including silcrete) or other in-

soluble silicates or dissolve resistant minerals such as chromites, rutile, cassiterite, ilmenite and zircon (Fletcher, 1981; Potts, 1987; Thompson and Walsh, 1989).

A rigorous quality control/analysis procedure was followed by inserting a field duplicate at baren quartz (blank). About 97% of the blank samples fell below the detection limit suggesting barely no contamination. Analysis of pair of samples using simple regression and half absolute relative deviation plots showed a coefficient of correlation of 15% indicating a very low precision. This may be due to the high heterogeneity and nugget effect of the paleo-placers. In this study, a total of 891 data points consisting of gold (Au) and positional coordinates (Easting, Northing, Elevation) in the Universal Transverse Mercator (UTM30N) projection system was obtained through field measurements and used. Table 1 presents the statistical description of the dataset.

Typically, as with all machine learning techniques, a very large dataset for computations is required in order to generalise globally and make very good predictions. This involves a method of fine-tuning at the training and testing phases. In this study, a structured procedure used in the final tuning of the model is to divide the dataset for training and testing purposes (Lantz, 2015; Kuhn and Johnson, 2013). Therefore, the entire 891 data points used in this study were partitioned into training (70%) and testing (30%) sets,

**Table 1**  
Summary statistics of the data.

Parameter	Sample point	Min.	Max.	Mean	Std. Dev.	Skewness	Kurtosis
Au (ppb)	891	4.00	23.00	7.71	2.87	1.86	4.79
Easting (m)	891	597,962.94	609,705.51	601,344.45	2200.90	1.53	2.48
Northing (m)	891	576,487.24	589,666.81	582,751.53	3206.33	0.13	-0.96
Elevation (m)	891	24.50	176.01	59.73	21.40	2.35	8.46

**Table 2**  
Test results of the various MARS models developed based on different orders of interactions.

Model Number	FBF	Order of Interaction	Training		Testing	
			MSE	R	MSE	R
1	30	0	1.6868	0.8827	1.8495	0.8973
2	30	1	0.7252	0.9513	0.9342	0.9495
3	30	2	0.6271	0.9581	0.7507	0.9596
4	30	3	0.6271	0.9581	0.7507	0.9596
5	50	0	1.5037	0.8962	1.8102	0.9000
6	50	1	0.5569	0.9629	0.7842	0.9578
7	50	2	0.5034	0.8725	0.6367	0.8704
8	50	3	0.5034	0.9664	0.6367	0.9659
9	60	0	1.4608	0.8992	1.7076	0.9056
10	60	1	0.5245	0.9650	0.7345	0.9605
11	60	2	<b>0.4785</b>	<b>0.9682</b>	<b>0.6070</b>	<b>0.9675</b>
12	60	3	0.4785	0.9682	0.6070	0.9675

representing 624 and 267 sets. The training set was used for the model building, while the testing set was applied to test or validate the performance of the trained model. It is important to note that there are no universally accepted criteria for splitting the dataset. Fig. 6 provides information on the model development phases.

To avoid the likelihood of potential overfitting or underfitting, the training data was carefully selected to give a representation of the study area. Hence, the training-testing data selection was made through the stratified hold-out random sampling procedure, which has been widely adopted in machine learning predictions (Saltelli et al., 2008; Hastie et al., 2009; Koyuncu and Kadilar, 2009; Koyuncu, 2013; Singh et al., 2015). During the preprocessing phase, the datasets were normalised to ensure constant variability and prevent being skewed by certain attributes with large values. This is valid due to differences in the range of physical quantities and units of the data set used. In this study, the dataset was normalised in the range of [0–1] using Eq. (19) (Mueller and Hemond, 2013):

$$N_i = a + \frac{[(x_i - A)(b - a)]}{B - A} \quad (19)$$

where  $N_i$  is the normalised data,  $a$  and  $b$  are minimum and maximum scales respectively, that are set at 0 and 1.  $x_i$  is the measured normalising data,  $A$  and  $B$  are the minimum and maximum data values of the entire dataset.

## 5.2. Proposed MARS model development

In this study, the input parameters were Easting (E), Northing (N) and Elevation (Z) and Au grade value was used as the output parameter in the MARS model development. In all, twelve different MARS models with varying basis functions were developed based on different piecewise order of interactions. In this study, the 0, 1st and 2nd order piecewise interactions were carried out. In the 0 order there is no interaction between predictor variables while for the 1st and 2nd orders, there are possible interactions between predictor variables up to two or more linear members. The essence of testing different orders of interactions is to determine the op-

timal MARS model whose prediction performance is greatly influenced by the order of interactions used. Table 2 presents the training and testing results of the various MARS models developed based on the different order of interactions and the total number of basis functions used at the forward stage designated as FBF. All the MARS models were trained with zero penalty and 3rd degree of freedom for knot optimisation.

Finally, the optimal MARS model was determined based on the premise that the model should attain the least RMSE, MARE and highest R values (Table 2). From Table 2, it can be observed that the R varied within 0.9500 and 0.9600 for the various MARS models. Slight overfitting was observed at zero interaction, predicting R values between 0.8827 and 0.9065. The MSE values were in the range 0.400 and 0.900 for the interactive models, and from 1.400 to 1.700 for zero-order interactions. Because all the interactive models gave an R value very close to 1 and an MSE value close to 0, suggest MARS capability to overcome complex geospatial relationships and accurately predict geochemical grades of placer deposits. The presence of interactions is so significant in building an accurate model for Au predictions and not simply additive. Again, it indicates that MARS has the capability to capture complex and nonlinear relationships of datasets without prior assumptions about the underlying functional relationship between the predictor variables and output response (Zhang, 2019).

The final optimal MARS model (Eq. (20)) at the forward phase had 60 basis functions (see Table 2), but after backward pruning (deleting redundant knots in a step-wise regression manner), an optimum 35 basis functions was achieved. The same results were produced by both the 2nd and 3rd orders interactions as shown in Table 2. Due to model performance and simplicity, the 2nd order was selected as the optimal MARS model with its respective equations shown in Table 3. Therefore, the piecewise 2nd order interaction which comprises of product between the predictor variables (E, N, Z) and basis functions, can be observed in Table 3. According to the training and testing results presented in Table 2, the MARS model has demonstrated its capability in accurately predicting regolith geochemical grade values in a paleo-placer environment. Furthermore, it is obvious that the MARS model has been able to

**Table 3**  
Details of the selected optimal MARS model.

$\beta_m$	Model Equation	Coefficients ( $h_m$ )	$\beta_m$	Model equation	Coefficients ( $h_m$ )
BF2	max(0, 0.733 - N)	44.71	BF31	max(0, E - 0.274) * BF18	352.04
BF4	max(0, 0.283 - Z)	-44.41	BF32	max(0, 0.274 - E) * BF18	-106.58
BF5	max(0, E - 0.868) * BF4	-181.96	BF33	max(0, Z - 0.336) * BF8	-1616.76
BF6	max(0, 0.868 - E) * BF4	90.98	BF35	max(0, N - 0.329) * BF28	-577.65
BF7	max(0, E - 0.278) * BF1	449.27	BF37	max(0, N - 0.537) * BF28	-1420.61
BF9	max(0, N - 0.303) * BF6	-196.41	BF40	max(0, 0.242 - N) * BF27	302.72
BF11	max(0, N - 0.304) * BF4	92.24	BF41	max(0, Z - 0.321)	26.93
BF13	max(0, E - 0.156) * BF2	-334.04	BF43	max(0, E - 0.182) * BF17	-346.01
BF14	max(0, 0.156 - E) * BF2	212.02	BF45	max(0, E - 0.362) * BF3	152.30
BF15	max(0, Z - 0.207) * BF1	73.14	BF46	max(0, 0.3620 - E) * BF3	33.39
BF17	max(0, N - 0.603)	37.23	BF47	max(0, Z - 0.164) * BF31	-288.12
BF19	max(0, E - 0.272)	38.15	BF48	max(0, 0.164 - Z) * BF31	657.35
BF20	max(0, 0.272 - E)	-38.52	BF51	max(0, N - 0.171) * BF49	191.74
BF21	max(0, Z - 0.611)	-35.06	BF52	max(0, 0.171 - N) * BF49	-268.67
BF23	max(0, E - 0.375) * BF15	-1681.24	BF54	max(0, 0.409 - E) * BF12	-607.00
BF29	max(0, N - 0.510) * BF28	2410.75	BF55	max(0, E - 0.544)	7.18
BF30	max(0, 0.510 - N) * BF28	-760.57	BF57	max(0, Z - 0.472) * BF56	-51.37
			BF60	max(0, 0.283 - N) * BF42	-75.54

**Table 4**  
Comparison of MARS model and other machine learning methods testing results.

Method	Performance criteria			
	R	RMSE	MAE	$\rho$
MARS	0.9675	0.7791	0.6481	0.0497
BPNN	0.9665	0.7920	0.6585	0.0506
RBFNN	0.9616	0.8766	0.7683	0.0561
GRNN	0.9435	1.0236	0.8106	0.0661

learn the complex relationship existing between the regolith geochemical characteristics with gold (Au) values. Hence Eq. (20) can intuitively generalise correctly for un-sampled prospective areas with high accuracy.

$$Au = 4.12429 + \sum_{m=1}^{35} \beta_m h_m(x) \quad (20)$$

### 5.3. Comparison of MARS model and other investigated techniques

The applied BPNN, RBFNN and GRNN methods have over the years been extensively studied and applied in literature as benchmark techniques for comparison with other machine learning methods in geosciences and other related disciplines (Ziggah et al., 2016; Arthur et al., 2020; Poulton, 2002; Van der Baan and Jutten, 2000). Hence, the present authors saw it as an opportunity to apply and compare them to the proposed MARS technique. To test the strength of MARS with these benchmark machine learning methods, we selected the same datasets for training and testing. Table 4 presents a summary statistical performance comparison based on the testing data for the MARS, BPNN, RBFNN and GRNN.

From Table 4, the predicted R for the MARS model perfectly match the observed Au values within the study area (paleo-placer deposit) by 96.82%. This was closely followed by the BPNN, RBFNN and GRNN. In comparison to other artificial intelligence models, MARS has demonstrated its superiority against the other methods by its highest R value (Fig. 7). The RMSE and MAE have widely used performance measures in statistics to evaluate the closeness of a model prediction to the observed data (Willmott and Matsuura, 2005). Again, MARS demonstrated its predictive accuracy over the BPNN, RBFNN and GRNN methods with producing the

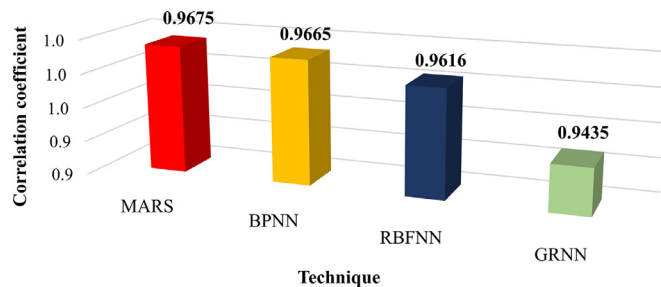


**Fig. 7.** Performance comparison of MARS and other machine learning techniques based on R.

least RMSE and MAE values (Table 4). A lower correlation index,  $\rho$  also indicates a more precise model. As observed from Table 4, the  $\rho$  value for the proposed MARS model produced 0.0497 while BPNN, RBFNN and GRNN predicted 0.0506, 0.0561 and 0.0661, respectively.

Based on the overall analyses, the proposed MARS model comparatively has the strongest calibration abilities. That is, given the testing dataset, the MARS exhibited an excellent prediction tendency than the other machine learning techniques investigated in this study. This can be attributed to the capability of the MARS to capture inherent complex high pattern relationships within predictor parameters amongst the training and the testing datasets (Zang and Goh, 2016).

Further, the optimum models of the MARS, BPNN, RBFNN and GRNN were compared with the classical kriging method. In order to create uniformity and consistency in comparison, the 891 datasets were used as testing datasets in the optimum trained MARS, BPNN, RBFNN and GRNN models. The kriging estimation was done through experimental variography modelling. The variography utilised a spherical model, twelve lags, and assumed anisotropy. Table 5 summarises the results based on MARS, BPNN, RBFNN, GRNN and the Kriging method. Interestingly, the proposed MARS approach achieved the best in all aspects of the performance indicators values indicated by a maximum R value and a minimum error (i.e., RMSE, MAE and  $\rho$ ). Graphical presentation of the predictive strength of the MARS technique against other techniques is shown in Fig. 8(a-d).

Fig. 9(a-e) compares the measured Au with the predicted models for all the methods investigated in this study. The plot shows an excellent correlation of the measured and the predicted Au

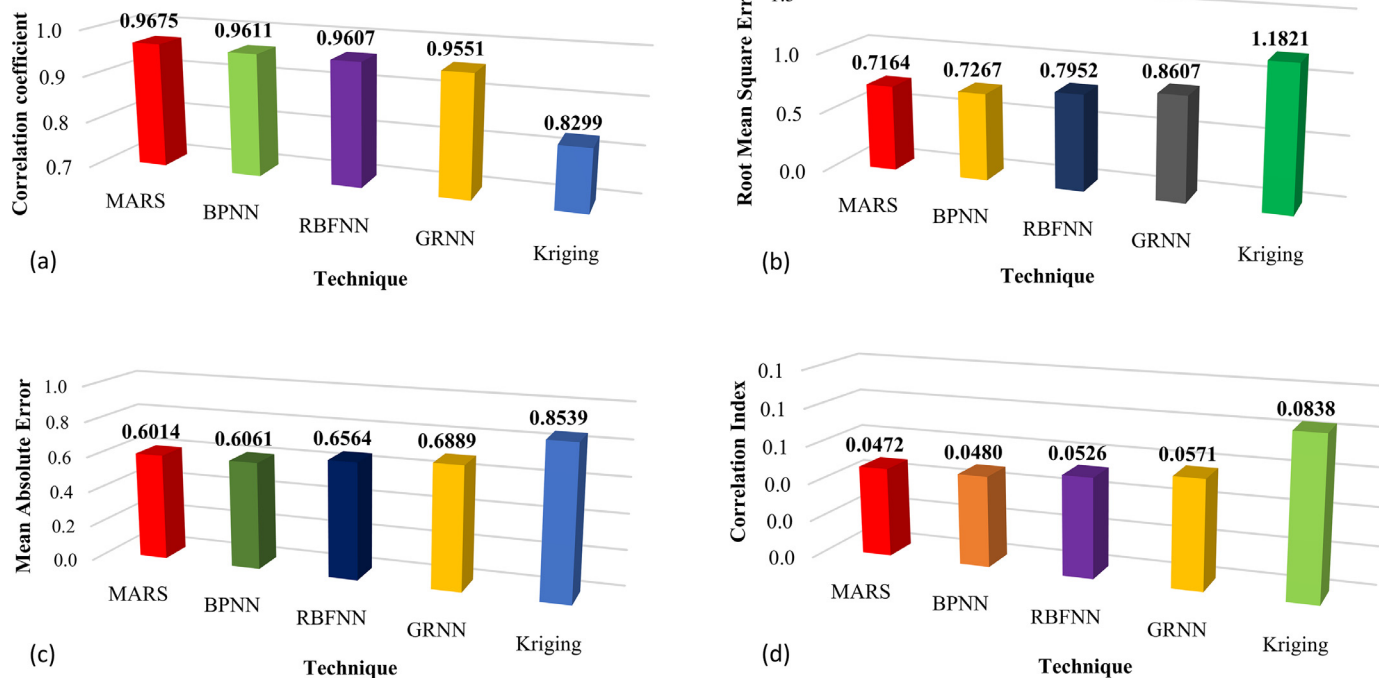


**Fig. 8.** Performance of the various techniques based on: (a)  $R$ ; (b) RMSE; (c) MAE; and (d) correlation index ( $\rho$ ).

**Table 5**  
Comparison of all developed models and performance indicators.

Method	Performance criteria (Accuracy for Testing sets)			
	RMSE	$R$	MAE	$P$
MARS	0.7164	0.9675	0.6014	0.0472
BPNN	0.7267	0.9611	0.6061	0.0480
RBFNN	0.7952	0.9607	0.6564	0.0526
GRNN	0.8607	0.9551	0.6889	0.0571
Kriging	1.1821	0.8299	0.8539	0.0838

for the MARS model, demonstrating its efficiency over the models. From Fig. 9(a), almost 96.7% of the variation of the measured Au (ppb) data is explained by the MARS model. This was closely followed by BPNN (96.5%), RBFNN (95.9%) and GRNN (94.6%) as shown in Fig. 9(b-d), respectively. However, OK achieved the least performance by only explaining 89.4% of the variation in the measured Au data as shown in Fig. 9(e). The MARS model produced similar estimates of the  $R$  value with the rest of the neural network models, and even generalised very well for extreme Au values.

Fig. 10 shows a combined line plot of the measured and predicted Au for all the models. It is worth noting that all the models show an excellent prediction at various ranges of sample index. This plot also reveals very interesting subtle information with respect to the performance of the machine learning models against the classical ordinary kriging methods. In comparison with the results obtained for the other methods, the MARS model gave an excellent prediction where the predicted Au values were more consistent with the observed values. This generalisation can be attributed to the better and more versatile learning capabilities of MARS models against the other models. In terms of regolith geochemical gold prediction, the authors with no doubt demonstrated MARS' remarkable performance against other machine learning models (GRNN, BPNN and RBFNN) and kriging geostatistical ap-

proaches. Indeed, these results indicated that the MARS model is better suited for Au prediction in the study area.

#### 5.4. Sensitivity and multicollinearity analysis

Sensitivity analysis was carried out to identify predictive variables that have a significant impact on the observed variable (Sorentino and Barnett, 1994). This further serves as quality assurance and contributes to the defensibility of model-based analysis (Saltelli et al., 2000; Saltelli et al., 2004; Saltelli et al., 2008). Statistical techniques used to test the significance of predictor variables are not well developed for artificial neural networks. One of the advantages of the MARS approach is its ability to make feature selections on the predictor variables. Hence, the sensitivity analysis was carried out using the MARS technique. To identify input predictor variables that participate in interactions with each other, MARS uses the ANOVA decomposition method. Fig. 11 shows the relative importance of the input parameters (Easting, Northing and Elevation) on the output (Au) in the model development process. According to Fig. 11, the UTM(N) parameter was selected as the dominant input parameter, which contributes to 100% of the predicted model. This was closely followed by Easting (88.14%) and Elevation (82.44%) respectively. By virtue of the sensitivity analysis results, it can also be deduced that all the input parameters contributed significantly to the model building.

Multicollinearity analysis was performed to determine how the input and output variables are correlated to each other. In diagnosing multicollinearity, the study used the Variance Inflation Factor (VIF) index (Stine, 1995; Akinwande et al., 2015) to measure how much the variance of an estimated regression coefficient has increased due to collinearity (Stine, 1995; Akinwande et al., 2015). The VIF (Eq. (21)) is mathematically expressed as:

$$VIF_m = \frac{1}{1 - R_m^2} \quad (21)$$

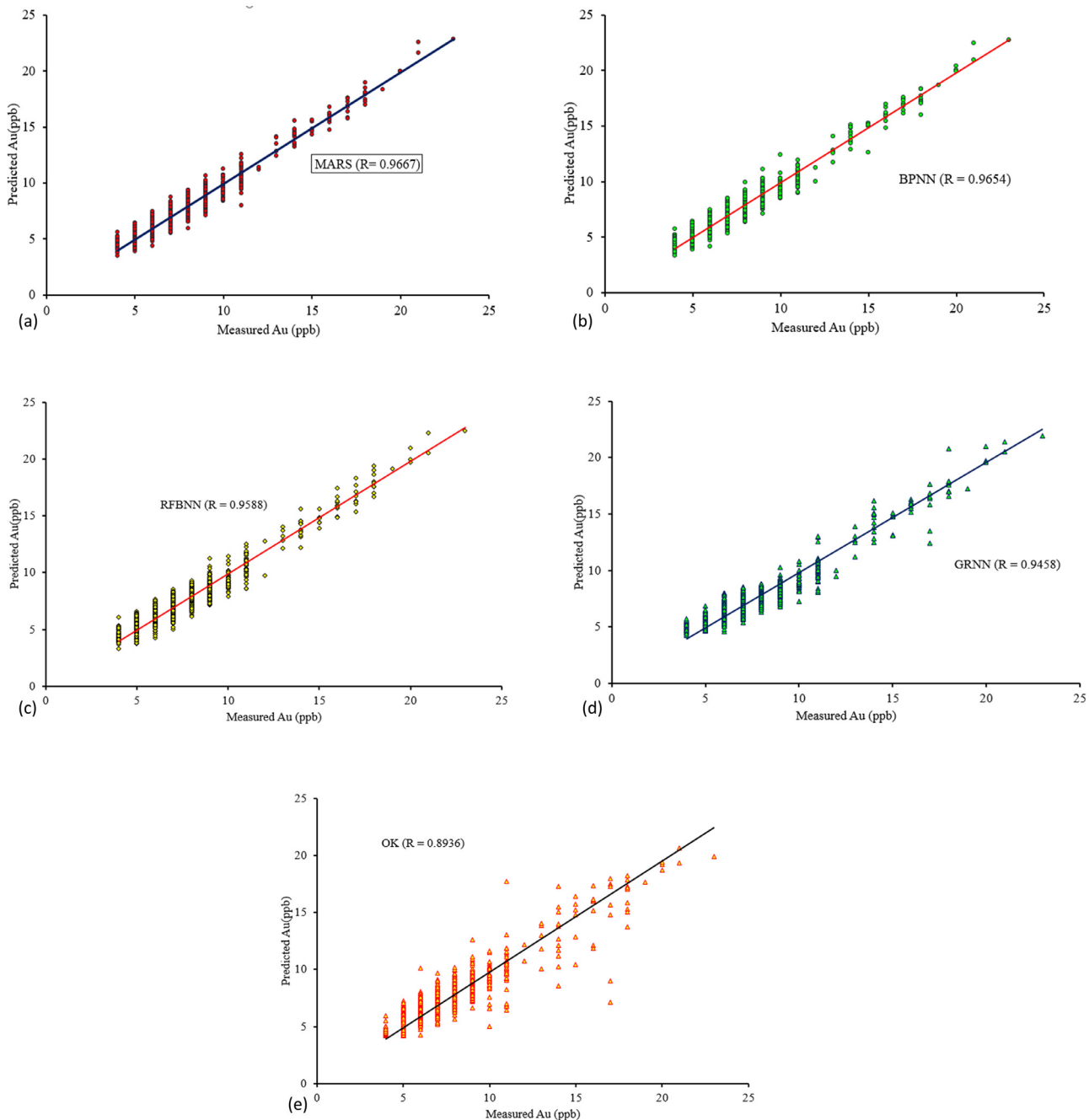


**Fig. 9.** Measured versus predicted Au (ppb) values using different models: (a) MARS; (b) BPNN; (c) RBFNN; (d) GRNN; and (e) OK.

**Table 6**  
Multicollinearity indexes for predictor variable.

Analysis	Easting coordinate	Northing coordinate	Elevation
Variance Inflation Factor	1.0031	1.0103	1.0201

where  $R^2$  of the  $m^{th}$  variable is the coefficient of determination obtained through regressing the input variables. Table 6 summarises the result of the VIF. VIF of 1 shows that none of the factors is correlated meaning there is no multicollinearity existing amongst the predictors. For moderately correlated factors, VIF should lie between 1 and 5. Moreover, if VIF is greater than 10, then the assumption is that the model coefficient is poorly estimated due

to strong multicollinearity. It can be observed from Table 6, that the Easting, Northing and Elevation coordinates (input parameters) produced a VIF of approximately 1. The interpretation is that these input parameters do not exhibit any multicollinearity amongst them but rather correlate well with the output parameter (Au). To this end, it can be stated that all three input parameters were suitable for use in the formulation of the various Au predictive models.

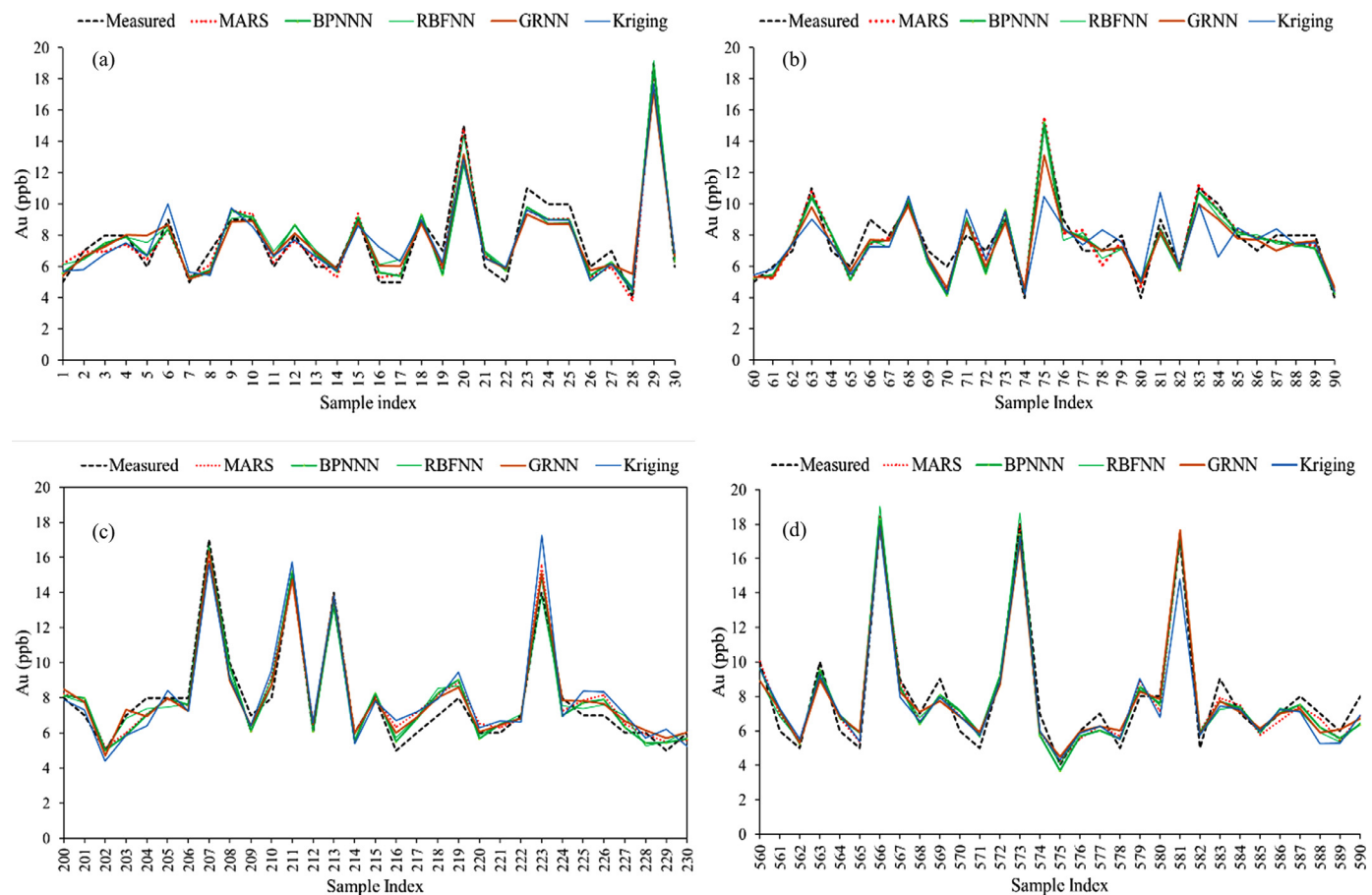


**Fig. 10.** Comparison of measured and predictive models of Au values by subsampling of (a) 1 up to 30; (b) 60–90; (c) 200–230; and (d) 560–590 samples.

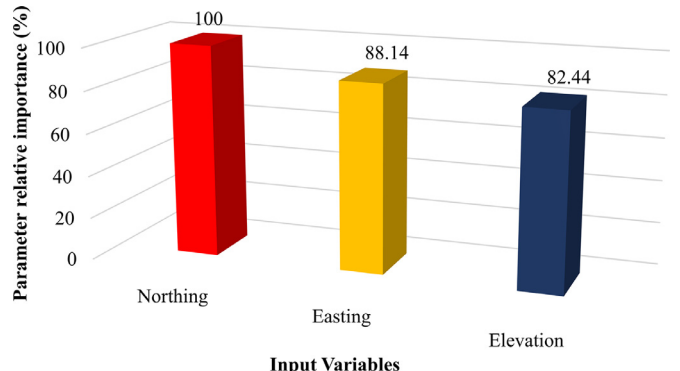


**Fig. 11.** Relative importance of the input variables.

## 6. Conclusions

Over the years, the empirical method of Kriging has been widely used for regolith geochemical grade estimation. A review of previous studies indicates that the Kriging approach oftentimes does not produce satisfactory results. Therefore, this study applied the MARS as a novel approach to regolith geochemical grade estimation within the Tarkwaian district. The proposed MARS approach was compared with three standard ANN methods (BPNN, RBFNN and GRNN) and empirical method (Kriging). These modelling techniques were applied to the regolith geochemical dataset to aid in accurate estimation and prediction of Au value within

the Tarkwaian paleoplacer deposit. The performance of the methods was evaluated using statistical indicators such as  $R$ , RMSE, MAE and  $\rho$ . The major findings are:

The statistical results revealed that the MARS technique gave superior results as compared to the BPNN, RBFNN, GRNN and Kriging. This was evident from the results where MARS had the lowest values of RMSE (0.7164), MAE (0.6014),  $\rho$  (0.0472) as well as highest  $R$  (0.9675) value.

It can be inferred from the reported results that the MARS approach can learn the intricacies and complex relationships existing between the regolith geospatial parameters ( $E$ ,  $N$  and  $Z$ ) with gold (Au) values. These results have shown that the proposed MARS approach is useful for predicting Au with some degree of certainty.

Furthermore, the sensitivity and multicollinearity test revealed that the geospatial input parameters were equally qualified to be used in the development of the predictive models.

Overall, the present study has provided clear insight into the strength and robustness of MARS in predicting Au anomalies in a highly complex regolith geochemical environment. The authors are intrigued by the performance of the MARS model and therefore has the exciting fervour to propose the MARS modelling technique. This outcome may prove quite useful for the mining and exploration industry when MARS could be an effective computational tool to unravel regolith geochemical complexities. This is because MARS has shown all the favourable characteristics to be adopted as a tool for the analysis of regolith geochemical datasets due to (a) its self-adaptive strength, (b) robust interactive variables, (c) computational efficiency and (d) accuracy and reliable predictions.

## Declaration of Competing Interest

The authors declare that they have no known competing financial interests or personal relationships that could have appeared to influence the work reported in this paper.

## Acknowledgements

The authors would like to thank Anglogold Ashanti Iduapriem, Tarkwa for providing the data and other logistics for the success of this research.

## References

- Abedi, M., Norouzi, G.H., Bahroudi, A., 2012. Support vector machine for multi-classification of mineral prospectivity areas. *Comput. Geosci.* 46, 272–283.
- Abraham, A., Steinberg, D., 2000. Is neural network a reliable forecaster on Earth? A MARS query!. *Bio-Inspired Applications of Connectionism*, 679–686. Lecture Notes in Computer Science No 2085 In: Mira, J., Priet, A.(Eds.. Springer Verlag Germany ISBN 3540422374.
- Afzal, P., Harati, H., Alghalandis, Y.F., Yasrebi, A.B., 2013. Application of spectrum-area fractal model to identify of geochemical anomalies based on soil data in Kahang porphyry-type Cu deposit Iran. *Chemie der Erde-Geochem.* 73 (4), 533–543.
- Ahmadian, A.S., 2016. *Numerical Models For Submerged Breakwaters Coastal Hydrodynamics and Morphodynamics*. Elsevier Oxford, p. 351.
- Akinwande, M.O., Dikko, H.G., Samson, A., 2015. Variance inflation factor: as a condition for the inclusion of suppressor variable(s) in regression analysis. *Open J. Stat.* 5 (7), 754–767 104236/ojs201557075.
- Allibone, A.H., McCuaig, T.C., Harris, D., Etheridge, M.A., Munroe, S., Byrne, D., Amanor, J., Gyapong, W., 2002. Structural controls on gold mineralization at the Ashanti gold deposit Obuasi Ghana. *Goldfarb, R.J., Neilson, R.L.(Eds. Integrated Methods for discovery: Global Exploration in the 21st Century* 9, 65–93.
- Arthur, C.K., Temeng, V.A., Ziggah, Y.Y., 2020. Multivariable Adaptive Regression Splines (MARS) approach to blast-induced ground vibration prediction. *Int. J. Min. Reclam. Environ.* 34, 198–222 101080/1748093020191577940.
- Asuero, A.G., Sayago, A., González, A.G., 2006. The correlation coefficient: an overview. *Crit. Rev. Anal. Chem.* 36, 41–59.
- Barnett, C.T., Williams, P.M., 2012. A radical approach to exploration: let the data speak for themselves! *Society of Economic geologist newsletter* 90, 11–17.
- Behnia, P., 2007. *Application of radial basis functional link networks to exploration for Proterozoic mineral deposits in Central Iran*. *Nat. Resour. Res.* 16, 147–155.
- Bishop, C.M., 1991. Improving the generalization properties of radial basis function neural networks. *Neural Comput.* 3, 579–588.
- Bishop, C.M., 1995. Training with noise is equivalent to Tikhonov regularization. *Neural Comput.* 7 (1), 108–116.
- Boher, M., Michard, A., Albarede, F., Rossi, M., Milési, J.P., 1992. Crustal growth in West Africa at ca. 21 Ga. *J. Geophys. Res.* 97 (B1), 345–369.
- Breiman, L., 2001. Statistical modeling: the two cultures. *Stat. Sci.* 16 (3), 199–231.
- Broomhead, D.S., Lowe, D., 1988. Multivariable functional interpolation and adaptive networks. *Complex Syst.* 2, 321–355.
- Brown, W.M., Gedeon, T.D., Groves, D.I., Barnes, R.G., 2000. Artificial neural networks: a new method for mineral prospectivity mapping. *Aust. J. Earth Sci.* 47, 757–770.
- Carranza, E.J.M., 2011. Analysis and mapping of geochemical anomalies using log ratio-transformed stream sediment data with censored values. *J. Geochem. Explor.* 110 (2), 167–185.
- Carranza, E.J.M., Hale, M., 1997. A catchment basin approach to the analysis of reconnaissance geochemical geological data from Albay Province Philippines. *J. Geochem. Explor.* 60 (2), 157–171.
- Carranza, E.J.M., Laborte, A.G., 2016. Data-driven predictive modeling of mineral prospectivity using random forests: a case study in Catanduanes Island (Philippines). *Nat. Resour. Res.* 25, 35–50.
- Carranza, E.J.M., Owusu, A., Hale, M., 2009. Mapping of prospectivity and estimation of number of undiscovered prospects for lode gold southwestern Ashanti Belt Ghana. *Int. Inst. For. Geo.-Inform. Sci. Earth Observ.* (ITC) 44, 915–938.
- Carranza, E.J.M., Sadeghi, M., 2010. Predictive mapping of prospectivity and quantitative estimation of undiscovered VMS deposits in Skellefte district (Sweden). *Ore Geol. Rev.* 38, 219–241.
- Chai, T., Draxler, R.R., 2014. Root mean square error (RMSE) or mean absolute error (MAE)? Arguments against avoiding RMSE in the literature. *Geosci. Model Dev.* 7, 1247–1250.
- Chang, E.I., Lippmann, R.P., 1993. A boundary hunting radial basis function classifier which allocates centers constructively. *Adv. Neural Inf. Process. Syst.* 5, 139–146.
- Chatterjee, S., Bandopadhyay, S., Machuca, D., 2010. Ore grade prediction using a genetic algorithm and clustering based ensemble neural network model. *Math. Geosci.* 42 (3), 309–326 101007/s1 1004-010-9264-y.
- Cheng, Q., 2007. Mapping singularities with stream sediment geochemical data for prediction of undiscovered mineral deposits in Gejiu Yunnan Province China. *Ore Geol. Rev.* 32 (1), 314–324.
- Chen, S., Cowan, C.N., Grant, P.M., 1991. Orthogonal least squares learning algorithm for radial basis function networks. *IEEE Trans. Neural Netw.* 2 (2), 302–309.
- Chen, C., He, B., Zeng, Z., 2014. A method for mineral prospectivity mapping integrating C4 5 decision tree weights-of-evidence and m-branch smoothing techniques: a case study in the eastern Kunlun Mountains China. *Earth Sci. Inform.* 7, 13–24.
- Chièls, J.P., Delfiner, P., 2011. *Geostatistics: Modeling spatial Uncertainty*. Wiley Series in Probability and Statistics, New York, p. 695 pp.
- Davis, D.W., Hirdes, W., Schaltegger, E., Nunoo, E.A., 1994. U/Pb age constraints on deposition and provenance of Birimian and goldbearing Tarkwaian sediments in Ghana West Africa. *Precambrian Res.* 67, 89–107.
- Dutta, S., Bandopadhyay, S., Ganguli, R., Misra, D., 2010. Machine learning algorithms and their application to ore reserve estimation of sparse and imprecise data. *J. Intell. Learn. Syst. Applica.* 2, 86–96.
- Ewusi, A., Ahenkorah, I., Kuma, J.S.Y., 2017. Groundwater vulnerability assessment of the Tarkwa mining area using SINTACS approach and GIS. *Ghana Mining J* 17, 18–30 10.4314/gm.v17i1.3.
- Fletcher, W.K., 1981. Analytical methods in geochemical prospecting. In: *Handbook of Exploration Geochemistry*. Elsevier, Amsterdam, p. 255 pp.
- Friedman, J., 1991. Multivariate adaptive regression splines (with discussion). *Ann. Stat.* 19, 1–141.
- Gandomi, A.H., Alavi, A.H., Mirzaheini, M.R., Nejad, F.M., 2011. Nonlinear genetic-based models for prediction of flow number of asphalt mixtures. *J. Mater. Civil Eng.* 23 (3), 248–263.
- Gandomi, A.H., Alavi, A.H., Ryan, C., 2015. *Handbook of Genetic Programming Applications*. Springer International Publishing, Switzerland, p. 589 101007/978-3-319-20883-1\_1.
- Ghandhi, S.M., Sarkar, B.C., 2016. *Mineral Exploration and Evaluation*. Cambridge University Press, UK, p. 4808.
- Ghezelbash, R., Maghsoudi, A., 2018. Comparison of U-spatial statistics and C-A fractal models for delineating anomaly patterns of porphyry-type Cu geochemical signatures in the Varzaghan district NW Iran. *Comptes. Rendus Geosci.* 350 (4), 180–191.
- Ghezelbash, R., Maghsoudi, A., Daviran, M., 2018. Prospectivity modeling of porphyry copper deposits: recognition of efficient mono-and multi-element geochemical signatures in the Varzaghan district NW Iran. *Acta Geochimica* 38, 131–144.
- Goovaerts, P., 1997. *Geostatistics For Natural Resources Evaluation*. Oxford University Press, New York, p. 483.
- Griffis, R.J., 1998. Explanatory notes-geological interpretation of geophysical data from South-Western Ghana. *Minerals Commission, Accra* 51.
- Griffis, R.J., Barning, K., Agezo, F.L., Akosah, F.K., 2002. Gold deposits of Ghana Minerals Commission Accra 438 pp.
- Hagan, M.T., Demuth, H.B., Beale, M.H., 1996. *Neural Network Design*. PWS Publishing Boston MA.
- Haldar, S.K., 2013. *Mineral Exploration Principles and Applications*. Elsevier Publication, p. 370.
- Hale, M., 2000. *Geochemical Remote Sensing of the Subsurface Handbook of Exploration Geochemistry*, 7. Elsevier, Amsterdam.
- Hale, M., Plant, J., 1994. *Drainage Geochemistry Handbook of Exploration Geochemistry*, 6. Elsevier, Amsterdam.
- Hannan, S.A., Manza, R.R., Ramteke, R.J., 2010. Generalized regression neural network and radial basis function for heart disease diagnosis. *Inter. Jour. of Comp. Appl.* 7 (13), 7–13 0975 – 8887.
- Harris, D., Zurcher, L., Stanley, M., Marlow, J., Pan, G., 2003. A comparative analysis of favorability mappings by weights of evidence probabilistic neural networks discriminant analysis and logistic regression. *Nat. Resour. Res.* 12, 241–255.
- Harris, J.R., Wilkinson, L., Heather, K., Fumerton, S., Bernier, M.A., Ayer, J., 2001. Application of GIS processing techniques for producing mineral prospectivity maps - A case study: mesothermal Au in the Swayze Greenstone Belt Ontario Canada. *Nat. Resour. Res.* 10, 91–124.
- Hasanipanah, M., Armaghani, D.J., Khamesi, H., Amniesh, H.B., Ghoraba, S., 2016. Several non-linear models in estimating air-overpressure resulting from mine blasting. *Eng. Comput.* 32 (3), 441–455.
- Hastie, T., Tibshirani, R., Friedman, J., 2009. *The Elements of Statistical learning: Data Mining Inference and Prediction*. Springer-Verlag, New York, p. 745.
- Haykin, S., 1994. *Neural Networks: A comprehensive foundation*. MacMillan College Publishing Co, New York.
- Haykin, S., 1999. *Neural Networks: A Comprehensive Foundation*, 2nd edition Prentice Hall Englewood, Cliffs NJ.
- Hirdes, W., Senger, R., Adjei, J., Efa, E., Loh, G., Tettey, A., 1993. Explanatory notes for the Geological Map of Southwest Ghana - 1:100000 (Wiaviso Asafo Kukum Sunyani and Berekum sheets). *Geol. Jahrbuch Reihe B Heft* 83, 139.
- Ibrahim, B., Majeed, F., Ewusi, A., Ahenkorah, I., 2021. Residual geochemical gold grade prediction using extreme gradient boosting. *Environmental Challenges* 6, 100421.
- Isaaks, E., Srivastava, R.M., 1988. Spatial continuity measures for probabilistic and deterministic geostatistics. *Math. Geol.* 20 (4), 313–341.
- Isaaks, E.H., Srivastava, R.M., 1989. *An Introduction to Applied Geostatistics*. Oxford University Press, New York, p. 561.
- Junner, N.R., 1940. *Geology of the Gold Coast and Western Togoland (with revised geological map)* Gold Coast. Geolog. Surv. Bull. 11, 40.
- Karlik, B., Olgac, A., 2010. Performance analysis of various activation functions in generalized MLP architectures of neural networks. *Int. J. Artif. Intell. Expert Syst. (IJAE)* 1 (4), 111–122.
- Kapageridis, I.K., Derby, B., 1998. Neural network modelling of ore grade spatial variability. In: *Proceedings of the International Conference for Artificial Neural Networks (ICANN)*, 1. Springer-Verlag Skovde.

- Kesse, G.O., 1985. The Mineral and Rock Resources of Ghana. Balkema Publishers Rotterdam, p. 610.
- Keyan, X.N.L., Porwal, A., Leon, E.J.H., Lu, B., Y., 2015. GIS-based 3D prospectivity mapping: a case study of Jiama copper-polymetallic deposit in Tibet China. *Ore Geol. Rev.* 101016/joregeorev201503001.
- Koyuncu, N., 2013. Families of estimators for population mean using information on auxiliary attribute in stratified random sampling. *Gazi. Univ. J. Sci.* 26 (2), 181–193.
- Koyuncu, N., Kadilar, C., 2009. Family of estimators of population mean using two auxiliary variables in stratified random sampling. *Commun. Stat. Theory Method.* 38 (14), 2398–2417.
- Kuhn, M., Johnson, K., 2013. Applied Predictive Modeling. Springer Science Business Media, New York, p. 615 101007/978-1-4614-6849-3.
- Lantz, B., 2015. Machine Learning with R. Birmingham, p. 452 B3 2PB U.
- Leathwick, J.R., Elith, J., Hastie, T., 2006. Comparative performance of generalized additive models and multivariate adaptive regression splines for statistical modelling of species distributions. *Ecol. Model.* 19 (9), 188–196.
- Leathwick, J.R., Rowe, D., Richardson, J., Elith, J., Hastie, T., 2005. Using multivariate adaptive regression splines to predict the distributions of New Zealand's freshwater diadromous fish. *Freshw. Biol.* 50, 2034–2052.
- Liu, Y., Zhou, K., Carranza, E.J.M., 2018. Compositional balance analysis for geochemical pattern recognition and anomaly mapping in the western Junggar region China. *Geochemistry: exploration Environment. Analysis* 18 (3), 263–273.
- Loh, G., Hirdes, W., 1996. Explanatory Notes for the Geological Map of Southwest Ghana - 1:100000 scale (Axim and Takoradi sheets) Ghana. *Geol. Surv. Bull.* 49, 63 Accra.
- Mahmoudabadi, H., Izadi, M., Menhaj, M.D., 2009. A hybrid method for grade estimation using genetic algorithm and neural networks. *Computational Geosciences* 13, 91–101.
- Marjoribanks, R., 2010. Geological Methods in Mineral Exploration and Mining, 2nd edition Springer-Verlag, Berlin Heidelberg 101007/978-3-540-74375-0\_2.
- Milani, G., Benasciutti, D., 2010. Homogenized limit analysis of masonry structures with random input properties Polynomial response surface approximation and Monte Carlo simulations. *Struct. Eng. Mech.* 34 (4), 417–445.
- Misra, D., Samanta, B., Dutta, S., Bandopadhyay, S., 2007. Evaluation of artificial neural networks and kriging for the prediction of arsenic in Alaskan bedrock-derived stream sediments using gold concentration data. *Int. J. Min. Reclam. Environ.* 21 (4), 282–294 101080/17480930701259294.
- Moisen, G.G., Frescino, T.S., 2002. Comparing five modeling techniques for predicting forest characteristics. *Ecol. Modell.* 157, 209–225.
- Moody, J., Darken, C.J., 1989. Fast learning in networks of locally-tuned processing units. *Neural Comput.* 1, 281–294.
- Moyeed, R.A., Papritz, A., 2002. An empirical comparison of Kriging methods for nonlinear spatial point prediction. *Math. Geol.* 34, 365–386.
- Mueller, A.V., Hemond, H.F., 2013. Extended artificial neural networks: incorporation of a priori chemical knowledge enables use of ion selective electrodes for in-situ measurement of ions at environmentally relevant levels. *Talanta* 117, 112–118.
- Mueller, J.P., Massaron, L., 2016. Machine Learning for Dummies. John Wiley & Sons Inc Hoboken, New Jersey, p. 435.
- Musavi, M., Ahmed, W., Chan, K., Faris, K., Hummels, D., 1992. On the training of radial basis function classifiers. *Neur. Netw.* 5, 595–603.
- Nekoukar, V., Beheshti, M.T.H., 2010. A local linear radial basis function neural network for financial time series forecasting. *Appl. Intell.* 33 (3), 352–356 101007/s10448-009-0171-1.
- Nykänen, V., 2008. Radial basis functional link nets used as a prospectivity mapping tool for orogenic gold deposits within the Central Lapland Greenstone Belt Northern Fennoscandian Shield. *Nat. Resour. Res.* 17, 29–48.
- Oberthür, T., Vetter, U., Davis, D.W., Amanor, J.A., 1998. Age constraints on the gold mineralization and Paleoproterozoic crustal evolution in the Ashanti Belt of southern Ghana. *Precambrian Res.* 89, 129–143.
- Oh, H.J., Lee, S., 2010. Application of artificial neural network for gold-silver deposits potential mapping: a case study of Korea. *Nat. Resour. Res.* 19, 103–124.
- Parsa, M., Maghsoudi, A., Ghezelbash, R., 2016. Decomposition of anomaly patterns of multi-element geochemical signatures in Ahar area NW Iran: a comparison of U-spatial statistics and fractal models. *Arab. J. Geosci.* 9, 1–16.
- Patra, A., Das, S., Mishra, S.N., Senapati, M.R., 2015. An adaptive local linear optimized radial basis functional neural network model for financial time series prediction. *Neur. Comput. Appl.* 101007/s00521-015-2039-0.
- Perrotuy, S., Aillères, L., Jessell, M.W., Baratoux, L., Bourassa, Y., Crawford, B., 2012. Revised Eburnean geodynamic evolution of the gold-rich southern Ashanti Belt Ghana with new field and geophysical evidence of pre-Tarkwaian deformations. *Precambrian Res.* 204–205, 12–39.
- Pigois, J.P., Groves, D.I., Fletcher, I.R., McNaughton, N.J., Snee, L.W., 2003. Age constraints on Tarkwaian palaeoplacer and lodegold formation in the Tarkwa-Damang district SW Ghana. *Miner. Deposita* 38, 695–714.
- Poggio, T., Girosi, F., 1990. Networks for approximation and learning. *Proceed. IEEE* 78, 1481–1497.
- Porwal, A., Carranza, E.J.M., Hale, M., 2003. Artificial neural networks for mineral-potential mapping: a case study from Aravalli Province Western India. *Nat. Resour. Res.* 12, 155–171.
- Porwal, A., Carranza, E.J.M., Hale, M., 2004. A Hybrid neuro-fuzzy model for mineral potential mapping. *Math. Geol.* 36 (7), 803–826.
- Porwal, A., Gonzalez-Alvarez, I., Markwitz, V., McCuaig, T., Mamuse, A., 2010. Weights-of-evidence and logistic regression modelling of magnetic nickel sulfide prospectivity in the Yilgarn Craton Western Australia. *Ore Geol. Rev.* 38, 184–196.
- Potts, P.J., 1987. A Handbook of Silicate Rock Analysis. Blackie Glasgow, p. 622.
- Poulton, M.M., 2002. Neural networks as an intelligence amplification tool: a review of applications. *Geophysics* 67, 979–993 101190/11484539.
- Powell, M.J.D., 1977. Restart procedures for the conjugate gradient method. *Math. Program.* 12 (1), 241–254 101007/bf01593790.
- Quirós, E., Felicísimo, A.M., Cuartero, A., 2009. Testing Multivariate Adaptive Regression Splines (MARS) as a method of land cover classification of TERRA-ASTER satellite images. *Sensors* 9, 9011–9028 103390/s91109011.
- Reddy, R.K.T., Bonham-Carter, G.F., 1991. A decision-tree approach to mineral potential mapping in Snow Lake area Manitoba. *Canadian Journal of Remote Sensing* 17, 191–200.
- Rodríguez, G.V., Sanchez-Castillo, M., Chica-Olmo, M., Chica-Rivas, M., 2015. Machine learning predictive models for mineral prospectivity: an evaluation of neural networks random forest regression trees and support vector machines. *Ore Geol. Rev.* 71, 804–818.
- Rossi, M.E., Deutsch, C.V., 2014. Mineral Resource Administration. Springer Dordrecht Heidelberg, New York London, p. 337.
- Roy, A.S.G., Miranda, R., 1995. An algorithm to generate radial basis function (RBF)-like nets for classification problems. *Neur. Netw.* 8 (2), 179–201.
- Samanta, B., Bandopadhyay, S., 2009. Construction of a radial basis function network using an evolutionary algorithm for grade estimation in a placer gold deposit. *Comput. Geosci.* 35 (8), 1592–1602.
- Samanta, B., Bandopadhyay, S., Ganguli, R., 2004. Data segmentation and genetic algorithms for sparse data division in Nome placer gold grade estimation using neural network and geostatistics. *Min. Explor. Geol.* 11 (1–4), 69–76.
- Saltelli, A., Tarantola, S., Campolongo, F., 2000. Sensitivity analysis as an ingredient of modelling. *Statist. Sci.* 15 (4), 377–395.
- Saltelli, A., Tarantola, S., Campolongo, F., Ratto, M., 2004. Sensitivity Analysis in Practice: A Guide to Assessing Scientific Models. John Wiley & Sons Ltd, New York, p. 232.
- Saltelli, A., Ratto, M., Andres, T., Campolongo, F., Cariboni, J., Gatelli, D., Saisana, M., Tarantola, S., 2008. Global Sensitivity Analysis. The Primer John Wiley & Sons Ltd, New York, p. 305.
- Savaux, V., Bader, F., 2015. Mean square error analysis and linear minimum mean square error application for preamble-based channel estimation in orthogonal frequency division multiplexing/offset quadrature amplitude modulation systems. *IET Commun.* 9 (14), 1763–1773.
- Senapati, M.R., Dash, P.K., 2013. Intelligent system based on local linear wavelet neural network and recursive least square approach for breast cancer classification. *Artif. Intell. Rev.* 39, 151–163 101007/s10462-011-9263-5.
- Singh, H.P., Sharma, N., Tarry, T.A., 2015. An efficient class of two-phase exponential ratio and product-type estimators for estimating the finite population mean. *J. Stat. Appl. Prob. Lett.* 2 (1), 71–88.
- Skabar, A.A., 2005. Mapping mineralization probabilities using multilayer perceptrons. *Nat. Resour. Res.* 14, 109–123.
- Smith, P.L., 1982. Curve Fitting and Modeling With Splines Using Statistical Variable Selection Techniques. Langley Research Center Hampton Va Report NASA 166034.
- Sorentino, C., Barnett, D.W., 1994. Financial Risk and Probability Analysis in Mineral Valuation in Proceedings Mineral Valuation Methodology. Valmin '94 The Australasian Institute of Mining and Metallurgy Melbourne Australia, pp. 81–101.
- Srivastava, R.M., 1987. Minimum variance or maximum profitability. *CIMM* 80 (901), 63–68.
- Stine, R.A., 1995. Graphical interpretation of variance inflation factors. *Am. Stat.* 49, 53–56.
- Strebelle, S., 2002. Conditional simulation of complex geological structures using multiple-point geostatistics. *Math. Geol.* 34 (1), 1–22.
- Strogen, P., 1991. The sedimentology stratigraphy and structure of the Tarkwaian western region and its relevance to gold exploration and development. In: Proceedings of the International Conference on the Geology of Ghana Geological Society of Ghana Accra, 3, pp. R1–R39.
- Subramanian, N., Saraswathi, S., 2012. Barrister groupware (instant assistance to flawless law). *Bonfring Int. J. Softw. Eng. Soft Comput.* 2, 3437.
- Tahmasebi, P., Hezarkhani, A., 2009. Application of Optimized Neural Network by Genetic Algorithm. IAMG09 Stanford University California.
- Tahmasebi, P., Hezarkhani, A., 2010. Comparison of optimized neural network with fuzzy logic for ore grade estimation. *Aust. J. Basic Appl. Sci.* 4 (5), 764–772.
- Tahmasebi, P., Hezarkhani, A., 2012. A hybrid neural networks-fuzzy logic-genetic algorithm for grade estimation. *Comput. Geosci.* 42, 18–27.
- Taylor, N.P., Moorbat, S., Leube, A., Hirdes, W., 1992. Early Proterozoic crustal evolution in the Birimian of Ghana: constraints from geochronology and isotope geochemistry. *Precambrian Res.* 56, 97–111.
- Thompson, M., Walsh, N., 1989. Handbook of Inductively Coupled Plasma Spectrometry Blackie London USEPA 2000 Guidance for the Data Quality Objectives Process EPA QA/G4 EPA 600/R 096/055 Office of Environmental Information. Washington DC.
- Van der Baan, M., Jutten, C., 2000. Neural networks in geophysical applications. *Geophysics* 65, 1032–1047 101190/11444797.
- Willmott, C.J., Matsuura, K., 2005. Advantages of the mean absolute error (MAE) over the root mean square error (RMSE) in assessing average model performance. *Clim. Res.* 30 (1), 79–82.
- Yang, C.C., Prasher, S.O., Lacroix, R., Kim, S.H., 2003. A Multivariate Adaptive Regression Splines model for simulation of pesticide transport in soils. *Biosystems Eng.* B (1) 9–15.
- Yang, C.C., Prasher, S.O., Lacroix, R., Kim, S.H., 2004. Application of Multivariate Adaptive Regression Splines (MARS) to simulate soil temperature. *Trans. Am. Soc. Agric. Engrs.* 47 (3), 881–887.

- Yu, S., Zhu, K., He, Y., 2012. A hybrid intelligent optimization method for multiple metal grades optimization. *Neur. Comput. Applic.* 21, 1391–1402 101007/s00521-011-0593-7.
- Zang, W.G., Goh, A.T.C., 2016. Multivariate adaptive regression splines and neural network models for prediction of pile drivability. *Geosci. Front.* 7, 45–52 101016/jgsf201410003.
- Zhang, W., 2019. MARS Applications in Geotechnical Engineering Systems: Multi-Dimension with Big Data. Science Press and Springer Nature Singapore Pte. Ltd, p. 250 <https://doi.org/101007/978-981-13-7422-7>.
- Ziggah, Y.Y., Hu, Y., Yu, X., Basommi, L.P., 2016. Capability of artificial neural network for forward conversion of geodetic coordinates ( $\phi \lambda h$ ) to cartesian coordinates (x y z). *Math. Geosci.* 48 (6), 687–721 101007/s11004-016-9638-x.
- Zuo, R., 2017. Machine Learning of Mineralization-related Geochemical Anomalies: a review of potential methods. *Nat. Resour. Res.* 101007/s11053-017-9345-4.
- Zuo, R., Carranza, E.J.M., 2011. Support vector machine: a tool for mapping mineral prospectivity. *Comput. Geosci.* 37, 1967–1975.